crystals

MDPI

Review

Nanostructured Materials for Enhanced Performance of Solid Oxide Fuel Cells: A Comprehensive Review

Hicham Helal *, Mohammadi Ahrouch, Abdelaziz Rabehi, Dario Zappa and Elisabetta Comini *

Sensor Laboratory, University of Brescia, Via D. Valotti 9, 25133 Brescia, Italy; mohammadi.ahrouch@unibs.it (M.A.); abdelaziz.rabehi@unibs.it (A.R.); dario.zappa@unibs.it (D.Z.)
* Correspondence: h.helal@unibs.it (H.H.); elisabetta.comini@unibs.it (E.C.)

Abstract: Solid oxide fuel cells (SOFCs) have emerged as promising candidates for efficient and environmentally friendly energy conversion technologies. Their high energy conversion efficiency and fuel flexibility make them particularly attractive for various applications, ranging from stationary power generation to portable electronic devices. Recently, research has focused on utilizing nanostructured materials to enhance the performance of SOFCs. This comprehensive review summarizes the latest advancements in the design, fabrication, and characterization of nanostructured materials integrated in SOFC. The review begins by elucidating the fundamental principles underlying SOFC operation, emphasizing the critical role of electrode materials, electrolytes, and interfacial interactions in overall cell performance, and the importance of nanostructured materials in addressing key challenges. It provides an in-depth analysis of various types of nanostructures, highlighting their roles in improving the electrochemical performance, stability, and durability of SOFCs. Furthermore, this review delves into the fabrication techniques that enable precise control over nanostructure morphology, composition, and architecture. The influence of nanoscale effects on ionic and electronic transport within the electrolyte and electrodes is thoroughly explored, shedding light on the mechanisms behind enhanced performance. By providing a comprehensive overview of the current state of research on nanostructured materials for SOFCs, this review aims to guide researchers, engineers, and policymakers toward the development of high-performance, cost-effective, and sustainable energy conversion systems.

Keywords: SOFC; nanostructures; nanomaterials; electrochemistry; energy conversion; interfacial reactions; durability

Citation: Helal, H.; Ahrouch, M.; Rabehi, A.; Zappa, D.; Comini, E. Nanostructured Materials for Enhanced Performance of Solid Oxide Fuel Cells: A Comprehensive Review. *Crystals* **2024**, *14*, 306. https://doi.org/10.3390/cryst14040306

Academic Editor: Vladislav V. Kharton

Received: 23 February 2024
Revised: 20 March 2024
Accepted: 21 March 2024
Published: 26 March 2024

1. Introduction

The global quest for clean, sustainable, and efficient energy sources has gained a lot of attention due to concerns about the depletion of fossil fuels and the urgent need to address climate change [1]. Traditional energy sources, heavily reliant on fossil fuels, have shown limitations in terms of availability, environmental consequences, and long-term viability [2]. This growing awareness has prompted the exploration and development of alternative energy solutions, such as wind energy, solar cells, and fuel cells. Among these alternatives, fuel cells have emerged as promising candidates with significant potential to revolutionize the energy sector [3].

Fuel cells, first conceptualized by William Grove in 1838 [1], represent a transformative approach to energy conversion that has undergone comprehensive research and development over nearly seventeen decades, leading to significant advancements within the field. Unlike traditional power generation methods that involve combustion, fuel cells use electrochemical reactions to convert chemical energy directly into electricity. This intrinsic characteristic results in increased efficiency, reduced greenhouse gas emissions, and quiet operation [4]. In the spectrum of fuel cell technologies, the selection of electrolyte and fuel leads to the categorization into six different types of fuel cells such as polymer

electrolyte membrane (PEM), alkaline fuel cell (AFC), phosphoric acid fuel cell (PAFC), molten carbonate fuel cell (MCFC), solid oxide fuel cell (SOFC), and direct methanol fuel cell (DMFC) [3,5]. Table 1 provides a comparison among various fuel cell types regarding their operational temperature, power output, efficiency, and intended applications.

Table 1. Comparison of different types of fuel cells [6].

Fuel Cell Type	Operating Temperature (°C)	Power Range (kW)	Efficiency (%)	Application Brief
PEM	60–110	0.01–250	40–55	Portable, mobile, low power generation.
AFC	70–130	0.1–50	50–70	Mobile, space, military.
PAFC	175–210	50–1000	40–45	Medium to large scale power generation and CHP (Combined Heat and Power).
MCFC	550–650	200–100,000	50–60	Large scale power generation.
SOFC	500–1000	0.5–2000	40–72	Vehicle auxiliary power units, medium to large scale power generation and CHP, off-grid power and micro-CHP.
DMFC	70–130	0.001–100	40	Mobile, portable.

In recent developments, the integration of nanostructures and related phenomena has garnered attention for potentially enhancing SOFC performances. Nanostructured materials bring novel features, including increased surface area and improved catalytic properties, contributing to the efficiency and longevity of SOFCs. Investigations into nanostructure participation delve into phenomena like enhanced ion conductivity, reduced polarization losses, and improved electrochemical reactions within SOFCs. The intricate interplay of nanoscale features within the fuel cell architecture opens avenues for optimizing performance metrics, ultimately propelling SOFCs into more prominent roles within the energy landscape.

SOFC, characterized by its solid-state and robust materials, embodies a set of unparalleled attributes that make it a front-runner in the fuel cell ecosystem [7]. The presence of a solid electrolyte enables SOFCs to work at high temperatures. This high-temperature process leads to a series of advantages; the most important of them is the ability to use a wide range of fuels which include hydrocarbons, carbon monoxide, hydrogen, etc. [3,8]. Impressively, this versatility is achieved with minimal reliance on costly precious metal catalysts. Furthermore, the high operating temperature of SOFC applications produces excess waste heat that can be recycled as a cogeneration system. These cogeneration capabilities not only increase their efficiency but are also consistent with the broader goal of reducing resource waste and reducing environmental impact [9,10].

Despite their promise, the commercial viability of SOFCs hinges on overcoming challenges such as cost-effectiveness, durability, and integration into existing energy systems. Researchers are actively working towards addressing these hurdles and bridging the gap between innovation and practical application [11,12].

2. Working of SOFC

Solid oxide fuel cells (SOFCs) comprise an anode (fuel electrode), cathode (air electrode), and ion-conducting electrolyte [13], forming the core for converting chemical energy into electricity via electrochemical reactions. These reactions release electrons, which subsequently flow through an external circuit, generate an electric current that fuels the operation of the device [8]. The entire process is illustrated in Figure 1.

During the operational phase of a SOFC, the cathode becomes the site of oxygen introduction. In this setting, oxygen interacts with electrons, resulting in the creation of oxide ions [14], a process described by the equation:

$$O_2 + 4e^- \rightarrow 2O^{2-}. \quad (1)$$

These oxide ions cross the solid electrolyte by virtue of their inherent mobility and make their way toward the anode side. On the anode side, these oxide ions play a pivotal role in fuel oxidation, an essential step in the energy-generation process. For example, when hydrogen (H_2) serves as the fuel, the reaction proceeds as follows:

$$2O^{2-} + 2H_2 \rightarrow 2H_2O + 4e^-. \quad (2)$$

Similarly, if the fuel is methane (CH_4), the reaction became as follows:

$$2O^{2-} + CH_4 \rightarrow CO_2 + H_2O + 4e^-. \quad (3)$$

When carbon monoxide is present, the shift reaction, a chemical equilibrium process, occurs. This reaction involves the interaction between carbon monoxide (CO) and water (H_2O), leading to the formation of hydrogen gas (H_2) and carbon dioxide (CO_2). The equation representing this shift reaction is

$$CO + H_2O \rightleftharpoons H_2 + CO_2. \quad (4)$$

Given that carbon monoxide (CO) does not have a detrimental impact on the anode materials, it serves as an additional fuel source for the fuel cell. Furthermore, hydrocarbons can undergo internal reforming, as demonstrated by the following reaction:

$$C_xH_y + xH_2O \rightarrow xC_O + \left(x + \frac{y}{2}\right)H_2. \quad (5)$$

Reaction (5) typically does not reach chemical equilibrium in the anode, leading to the occurrence of the shift reaction (4), which results in additional hydrogen production. The comprehensive fuel cell reaction is expressed as follows:

$$H_2 + \frac{1}{2}O_2 \rightarrow H_2O. \quad (6)$$

The speed of the shift reaction (4) and the reforming process (5) is highly contingent on the catalysts used. These reactions release electrons, which subsequently flow through an external circuit, generating an electric current that fuels the operation of the device. The entire process is illustrated in Figure 1. For a complete review of the basics phenomena in SOFC, the reader is referred to [15].

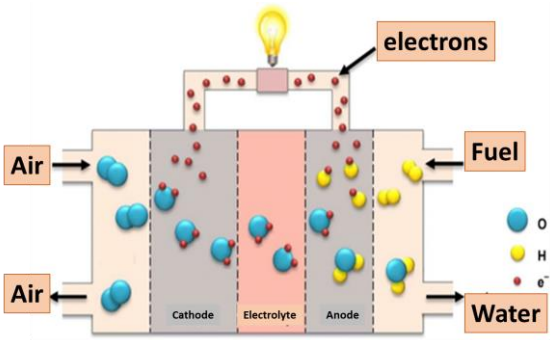

Figure 1. Working principle of solid oxide fuel cell. Reprinted with permission from Ref. [16], 2017, Elsevier.

3. SOFC Main Components

As previously mentioned, the SOFCs comprises three primary components: the anode, cathode, and electrolyte. To ensure efficient electricity generation, these components must possess specific attributes, including robust physical and chemical stability, compatibility with each other, strong mechanical strength with appropriate thermal expansion to prevent cell cracking, and cost-effectiveness [3,16]. Here, we will outline some of the critical properties of these SOFC components.

3.1. Electrolyte

The electrolyte serves as the core component within the cell unit, playing a pivotal role in determining the cell's performance. Its primary function involves the conduction of oxide ions from the cathode to the anode (or protons in the reverse direction), where they participate in reactions with the fuel (or oxidant gas), ultimately leading, for example, to the production of water or carbon dioxide. Additionally, it can provide structural support during the creation of high-temperature planar designs.

Electrolytes are typically classified into two types: single-layer and bilayer. In bilayer electrolytes, various materials are integrated to enhance the functioning of the SOFCs [1]. The design of an effective electrolyte for fuel cells encompasses several crucial considerations. First, it must exhibit high ionic conductivity while effectively insulating electronic flow [17]. A gas-tight structure, free from porosity, is essential to maintain the separation of gases within the cell, preventing leakage and preserving the desired electrochemical reactions. Achieving uniformly thin layers of the electrolyte is crucial to minimize ohmic losses, reducing energy losses within the cell. Moreover, matching the thermal expansion coefficient of the electrolyte with that of the anode and cathode materials is critical to prevent thermal stress and potential cell cracking [18,19]. Lastly, cost-effectiveness is a vital consideration, ensuring that the chosen electrolyte material meets performance requirements without significantly inflating production expenses, ultimately contributing to the commercial viability of fuel cell technology.

Yttria-stabilized zirconia (YSZ), scandia-stabilized zirconia (SSZ), gadolinium-stabilized zirconia (GSZ), cerium oxide (CeO_2), zirconium dioxide (ZrO_2), and bismuth oxide (Bi_2O_3) are among the various materials used as electrolytes. YSZ stands out as the most widely adopted [1,17,20], manufactured by all major fuel cell developers. These electrolytes demonstrate outstanding mechanical properties and high ionic conductivity, especially at elevated operating temperatures, typically around 800–1000 °C, all the while ensuring the cell's enduring stability and performance [21].

Studies have delved into YSZ's remarkable properties, showcasing its impressive ionic conductivity. Bagchi et al. [22], for instance, examined YSZ's ionic conductivity, achieving a maximum of 0.107 S cm^{-1} at 1000 °C, fabricated the using sol–gel method at a sintering temperature of 1200 °C. Additionally, Preux et al. [23] reported that YSZ's best ionic conductivity reaches 0.2 S cm^{-1} at 1000 °C with an 8 mol% yttrium oxide content. These findings highlight YSZ's potential for high-performance fuel cells.

However, challenges arise in applications requiring lower operating temperatures, prompting investigations into solutions such as reducing the thickness of YSZ electrolytes or introducing alternative oxide ion conductors with superior conductivity at lower temperature ranges.

3.2. Anode

Anodes in SOFCs play an essential role, encompassing several critical requirements to enable the efficient generation of electrical energy through fuel oxidation reactions. The anodes must exhibit high electronic conductivity and exceptional electrocatalytic activity to facilitate these reactions effectively. Operating within high-temperature reducing environments, anodes demand unwavering chemical stability to endure these harsh conditions [1].

The oxidation process takes place at the anode, necessitating a high level of electrocatalytic activity for fuel oxidation and for hydrocarbon reforming [8,24]. The anode conducts

the electrons released during the oxidation of hydrogen-containing fuel and uniformly distributes the fuel throughout its entire structure. The level of porosity within the anode is also of utmost importance as it enables the smooth transport of fuel to the reaction sites. Typically, the anode is crafted with a porosity ranging from 20% to 40% to facilitate the flow of gases [3].

Chemical compatibility is another vital consideration for anodes, especially their ability to withstand high temperatures without reacting with interconnects and electrolytes. To address this, the widely adopted approach is to employ nickel–yttria-stabilized zirconia (Ni-YSZ) as the anode material in SOFCs, often in combination with YSZ as the electrolyte. This combination excels due to nickel's remarkable conductivity and catalytic properties [17]. Furthermore, Ni-Gadolinium-doped ceria (Ni-GDC) has garnered significant attention as an anode material. Ni-GDC allows for relatively low-temperature SOFC operation while delivering outstanding physical and chemical attributes. When paired with GDC as the electrolyte, this combination has demonstrated exceptional performance at lower temperatures, expanding the possibilities for efficient operation across a broader range of conditions [3].

Moreover, novel metal–ceramic anode materials have emerged as a promising avenue, especially for SOFCs utilizing hydrocarbon fuels. These innovative anode materials incorporate alloying metals like Ni, Cu, Zn, Fe, among others, in combination with ceramic materials such as doped ceria or zirconia.

3.3. Cathode

The cathode, often referred to as the "oxygen electrode", in SOFCs plays a pivotal role in the electrochemical process, where it facilitates the reduction of oxygen gas to oxygen ions. Positioned opposite the anode within the SOFC assembly, it bears the critical role of catalyzing the transformation of oxygen molecules from the surrounding air into oxide ions [25].

For optimal performance, the cathode must possess high electronic and oxygen ion conductivity, a thermal expansion coefficient that matches that of the electrolyte, and sufficient porosity [26,27]. This porosity is essential to ensure the unimpeded flow of oxygen gas while also demonstrating chemical compatibility with the diverse components of the fuel cell [27]. Maintaining chemical stability, even under the extreme conditions of high-temperature, oxidizing environments, is non-negotiable to ensure the dependable operation of the cathode within the cell.

One widely used cathode material in high-temperature SOFCs is strontium-doped lanthanum manganite, often referred to as $La_{1-x}Sr_xMnO_3$ (LSM). LSM belongs to the manganite family of perovskites, with strontium partially substituting for lanthanum. This perovskite structure allows for various compositional and oxygen stoichiometry variations, optimizing catalytic and electrical properties. LSM is renowned for its exceptional electrical conductivity. Additionally, its thermal expansion coefficient closely matches that of the yttria-stabilized zirconia (YSZ) electrolyte, enhancing its suitability for SOFC applications and contributing to its widespread adoption [28].

As the operating temperature of the SOFCs decreases significantly, there is an observed increase in polarization resistance. This rise is attributed to the heightened activation energy (E_a) required for the oxygen reduction reaction (ORR) at lower temperatures, approximately 600 °C, rendering LSM unsuitable for deployment in the intermediate temperature (IT-SOFCs) range of 600–800 °C. In this pursuit, SOFCs featuring lanthanum strontium cobalt ferrite (LSCF) cathodes have been successfully developed, delivering consistent power outputs of 1.0–1.2 Wcm^{-2} at 800 °C and 0.7 V. Compared to conventional LSM cathodes, these advanced cathodes enable a reduction in operating temperature by approximately 100 °C while maintaining performance at the same level, thus offering promising prospects for IT-SOFC applications [29,30].

4. Proton-Conducting SOFC

Now that we have explored the conventional SOFC, let us delve into a fascinating variation known as the proton-conducting solid oxide fuel cell (PC-SOFC). A PC-SOFC is a type of fuel cell that operates at high temperatures and utilizes a proton-conducting electrolyte material instead of the conventional oxygen ion-conducting electrolyte. While both types of fuel cells share the same fundamental principle of converting chemical energy into electricity, they diverge in their choice of electrolyte material and operational parameters. PC-SOFC operates at intermediate temperatures [31] (typically between 500 °C and 700 °C) and employs a proton-conducting electrolyte instead of the more common oxygen-ion conducting electrolyte used in traditional SOFCs.

The electrochemical reactions occur at the anode, cathode, and electrolyte interfaces, facilitating the conversion of chemical energy into electrical energy. At the anode, typically composed of nickel or nickel–cermet materials, the fuel, often hydrogen (H_2) or hydrocarbons such as methane (CH_4), undergoes oxidation (reaction (7)):

$$H_2 \rightarrow 2H^+ + 2e^-. \quad (7)$$

Protons (H^+) are generated at the anode and migrate through the proton-conducting electrolyte material towards the cathode. Meanwhile, electrons (e^-) flow through the external circuit, creating an electrical current that can be utilized for power applications.

At the cathode, typically made of lanthanum strontium cobalt ferrite (LSCF) or similar mixed conducting materials [32–34], oxygen molecules from the air react with the migrating protons and electrons to form water (reaction (8)):

$$\frac{1}{2} O_2 + 2H^+ + 2e^- \rightarrow H_2O. \quad (8)$$

This reaction completes the circuit, providing a pathway for the electrons generated at the anode to recombine with the protons and oxygen molecules, forming water vapor as the primary reaction product.

Both PC-SOFCs and conventional SOFCs operate on the principle of electrochemical energy conversion, the type of electrolyte material used fundamentally changes the mechanisms of ion transport and electrochemical reactions. PC-SOFCs offer potential advantages in terms of performance and efficiency due to the faster kinetics of proton transport compared to oxygen ion transport, particularly in applications where lower operating temperatures are desirable for reduced material degradation and longer lifespan.

5. Cell Geometry

SOFCs come in several different cell designs, each with its unique characteristics and advantages. It can be divided into planar, tubular, flat-tubular, and monolithic, as illustrated in Figure 2.

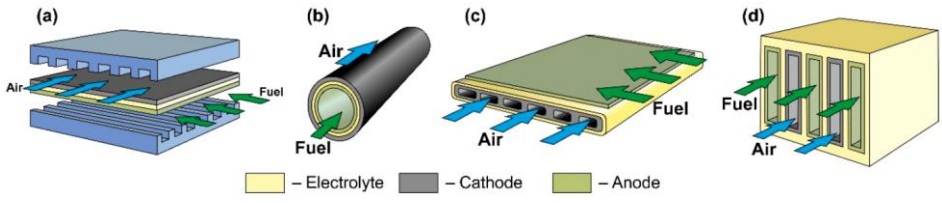

Figure 2. Illustrations of (**a**) planar, (**b**) tubular, (**c**) flat-tube, and (**d**) monolithic SOFC Designs. Reprinted with permission from Ref. [5], 2022, MDPI.

The planar configuration, as shown in Figure 2a, is highly preferred for its practical advantages [35]. It simplifies cell manufacturing and stack assembly, reduces costs, and allows for a high specific volumetric power by densely packing cells while minimizing electrical losses on connectors [1,5]. However, it does present challenges, such as the

complexity of achieving a hermetic seal between the anode and cathode chambers during stack assembly and limited resistance to thermal stress [36]. Consequently, there is a need for a redesigned SOFC design to address these issues effectively.

The second most popular SOFC design, illustrated in Figure 2b, is the tubular SOFC design [37], characterized by its cylindrical shape where the electrolyte tube functions as both the electrolyte and structural support for the cell. This design is renowned for its robust mechanical stability and resistance to thermal cycling [28]. Tubular SOFCs are often used in portable and small-scale applications. Nevertheless, tubular SOFCs exhibit a lower specific volumetric power when compared to planar cells because they have less densely packed cells and longer distances between cells in the stack. For a detailed comparison of properties between planar and tubular SOFCs, refer to the summary in Table 2. Furthermore, it is important to mention that the production of tubular cells tends to be more expensive [5].

Table 2. Comparison of tubular and planar SOFC properties.

Property	Tubular	Planar	Reference(s)
Power density	Lower	Higher	[38,39]
Volumetric power density	Lower	Higher	[40,41]
High temperature sealing	Easy	Difficult	[39]
Start-up and shut-down	Fast	Slow	[41]
Interconnector fabrication	Difficult	High cost	[39]
Fabrication cost	Higher	Lower	[42]
Fabrication simplicity	Difficult	Easy	[43]
Long-term stability	Excellent	Fair	[43]
Thermal cycling stability	Good	Fair	[40]

The flat-tube SOFC (FT-SOFC) design, depicted in Figure 2c, represents an ingenious amalgamation of planar and tubular SOFC architectures, offering a distinctive array of advantages. At its core, the FT-SOFC boasts an extruded anode support characterized by multiple cylindrical or semi-cyclical channels and ribs, shaping it into a flattened tube-like structure. These internal ribs serve a dual purpose as electron conductors; not only do they facilitate circumferential current flow, they also establish shorter and more efficient current pathways within the cell. This innovative design results in reduced ohmic resistance, ultimately translating into higher power density [44].

Beyond its superior electrical performance and power density, the FT-SOFC boasts attributes like straightforward gas-tight sealing, exceptional thermal durability, and ease of fabrication, making it a compelling candidate in the world of solid oxide fuel cell innovation [45,46].

The monolithic SOFC design, as depicted in Figure 2d, stands out with its distinctive arrangement of cell components within a corrugated structure. This flexible structure can be tailored to suit either gas co-flow or cross-flow configurations, offering versatility in its potential uses. Moreover, the MSOFC design frequently integrates an electrolyte support mechanism, a feature that contributes significantly to its stability and overall performance [47].

6. Electrochemical Mechanisms and Energy Losses

In theory, SOFCs represent an attractive prospect due to their operational adaptability, efficiency, and various advantages. However, the practical implementation of SOFCs faces many obstacles. Because of the numerous components and interfaces within the SOFC, understanding the physiochemical processes taking place at each cell location is exceedingly complex and critical to optimize performance and maximize efficiency. This necessitates in-depth research into reaction mechanisms and kinetics at various points

such as electrodes, electrolytes, and electrode–electrolyte interfaces, as well as identifying degradation mechanisms.

When an electrode becomes polarized, because of the electrochemical reactions taking place at its surface, an electric current is generated and flows through the external circuit. The level of this current is regulated by the interplay between the reaction kinetics and the diffusion of the reactants, including their movement toward and away from the electrodes.

In an ideal reversible fuel cell, the potential work that can be accomplished by electrons corresponds to the Gibbs free energy of the oxidation reaction, which is denoted by ΔG_{rxn}. This relationship is related to the oxygen fugacity's (or partial pressures) at the anode and cathode through Equation (9).

$$\Delta G_{rxn} = RT\, ln[P(O_{2\ ,anode})/P(O_{2\ ,cathode})] \tag{9}$$

$P(O_{2\ ,anode})$ represents the fugacity achieved through equilibrium with the H_2 and H_2O existing within the anode compartment.

Upon substituting the appropriate equilibrium expression for $P(O_{2\ ,anode})$ and converting to electrical units, Equation (9) becomes the Nernst equation, Equation (10).

$$V_{Nernst} = V^0 + \frac{RT}{nF}\, ln\left(\frac{P_{H_2\ ,\ anode}.\ P_{O_2,\ cathode}^{\frac{1}{2}}}{P_{H_2O\ ,anode}}\right) \tag{10}$$

where,

V^0 is the equilibrium potential at standard conditions,
n is the number of electrons taking part in each half-cell reaction,
F is Faraday's constant, the number of coulombs in a mole of electrons.

When using H_2 as the operating fuel, the cell's open-circuit potential, in the presence of a YSZ electrolyte, typically closely approximates the Nernst potential as calculated by Equation (5). In contrast, certain electrolytes like doped ceria, composed of cerium dioxide, exhibit a combination of both ionic and electronic conductivity known as mixed ionic and electronic conductivity (MIEC). This characteristic results in a reduction in the open-circuit voltage (OCV).

When electric current passes through the cell, it leads to a reduction in cell potential due to irreversible reactions occurring in the electrolyte and electrodes. This reduction in potential results in the generation of heat as a consequence of the lost energy. For electrolyte part, analyzing losses is a relatively simple task because each material naturally exhibits a certain level of conductivity. This inherent conductivity enables us to calculate the area-specific resistance (R_E) by considering both the material's conductive properties and the thickness of the electrolyte layer [48]. The energy loss within the electrolyte due to a current is equal to $i.R_E$, and it can be minimized by selecting an appropriate temperature and employing thin layers of electrolyte.

For the electrodes, they require materials with excellent electronic conductivity, resulting in minimal $i{\cdot}R$ voltage drops. Nonetheless, the transportation of gaseous reactants to the interface of the electrolyte, coupled with the slow kinetics of the electrode reactions, may result in voltage reductions known as electrode overpotentials, denoted as η_{anode} and $\eta_{cathode}$.

The variation of the cell potential with the current density is described by Equation (11):

$$V = V_{Nernst} - (iR_E + \eta_{anode} + \eta_{cathode}). \tag{11}$$

During low current density, the decrease in voltage primarily arises from constraints in electrochemical reaction rates, often denoted as activation polarization. At intermediate levels of current density, the cell experiences primarily ohmic losses, which arise from ionic and electronic resistance. These resistors have a linear effect on voltage drop as current density increases. When the current density reaches sufficiently high levels, there will be a

rapid decline in voltage. This phenomenon is the result of a process known as concentration polarization. When the current density reaches a sufficiently high level, gases are consumed within the cell more rapidly than the fuel or oxidant can contact the cell's surface, resulting in concentration polarization.

The resistance within a cell is the cumulative result of several contributing factors as described in the Equation (12):

$$R_{measured} = R_{electrolyte} + R_{cathode} + R_{anode} + R_{concentation}, \quad (12)$$

where,

$R_{electrolyte}$ is the resistance of the electrolyte,
$R_{cathode}$ is the ohmic and electrochemical losses at the cathode,
R_{anode} is the ohmic and electrochemical losses at the anode,
$R_{concentation}$ denotes the diffusion and gas conversion losses at the anode and cathode.

Numerous research studies [49–54] have been conducted to explore the potential of nanostructures in SOFCs to enhance electrochemical processes and mitigate energy loss. The nanostructures enhance the efficiency and performance of SOFCs through their minute dimensions and high surface area-to-volume ratio. Nanostructures facilitate faster ion and electron transport kinetics, thereby promoting more efficient electrochemical reactions within the SOFC. By precisely controlling the morphology and composition of nanostructured components such as electrodes and electrolytes, researchers can mitigate the ohmic and polarization losses that typically occur in conventional materials. This reduction in energy loss translates to improved overall efficiency and performance of the SOFC system.

7. Nanostructured Approaches in SOFC Engineering

It is widely recognized that achieving a high power density necessitates the total area-specific resistance of the electrolyte, anode, and cathode to be as low as possible [48]. Considering this, one strategy for enhancing properties and performance involves dividing the electrode into two distinct layers: (i) a thick conductive layer designed with significant porosity to enhance reactant diffusion and high conductivity to minimize ohmic losses; and (ii) a thin functional layer, approximately 5 to 10 µm thick, located in contact with the electrolyte (see Figure 3). This functional layer has the specific aim of improving the electrochemical reactions, featuring just the right balance of conductivity and porosity to reduce potential drops across its thickness to a minimum. The improvement of the electrochemical reactions is due to the extension of the triple phase boundary (TPB), where electrochemical reactions can occur, provided that there is a coexistence of gas-reactant molecules, electrons, and oxygen anions.

Another strategy for increasing and extending the TPB is the nano structuration of the electrode materials. Nanomaterials possess a high surface-to-volume ratio due to their nanoscale dimensions. When incorporated into the electrode structures of SOFCs, such as the cathode or anode, they significantly increase the available surface area for electrochemical reactions to take place. This increased surface area directly translates to more active sites for oxygen reduction at the cathode and fuel oxidation at the anode, thereby enhancing the cell's performance.

For instance, nano-sized particles or thin films can be used to coat the electrode surfaces, creating a highly porous structure with a larger TPB surface area compared to conventional microstructured electrodes. This increased surface area allows for greater contact between the electrode materials and the electrolyte, promoting faster ion and electron transport across the interface.

Furthermore, nanostructured electrolytes have been developed to reduce ionic resistance and enhance the ionic conductivity of the electrolyte material [55]. This improvement facilitates faster oxygen ion transport across the electrolyte, thereby reducing polarization losses and increasing the overall efficiency of the SOFC.

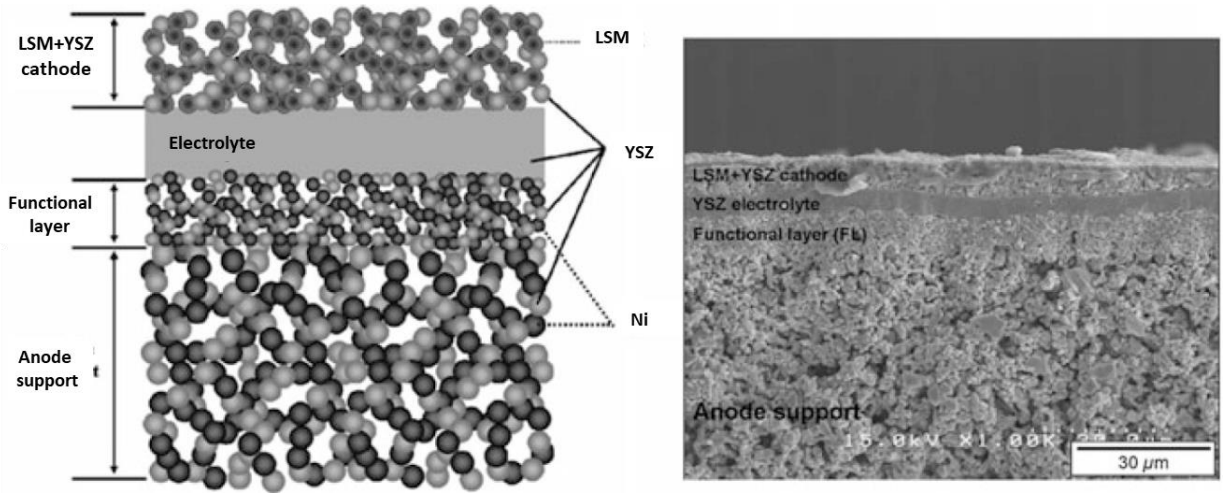

Figure 3. SOFC with an anode support created using tape-casting techniques and an additional anode functional layer. Reprinted with permission from Ref. [56], 2007, Elsevier.

7.1. Triple Phase Boundary

The necessity of all three components, a gas-phase molecule, electrons, and oxygen ions, coexisting concurrently is evident from the electrode reactions described in Equations (1) and (2) or (3). When the electrode material exclusively conducts electrons and the electrolyte solely conducts ions, these three species can only converge at the three-phase boundary (TPB) line. This line represents the point of contact between the electrode, the electrolyte, and the gas phase [57].

Maximizing the length of TPB can be accomplished by utilizing metal and ceramic composites, known as cermets. In these cermets, metallic catalysts and ionic conductors are combined in the correct proportion to achieve reciprocal percolation. This approach ensures that all the metals are effectively linked, facilitating the flow of electrons from the reaction sites to the external circuit. Additionally, there will be structures resembling "fins" that aid in the transfer of ions from the electrolyte to the electrode, as illustrated in Figure 4.

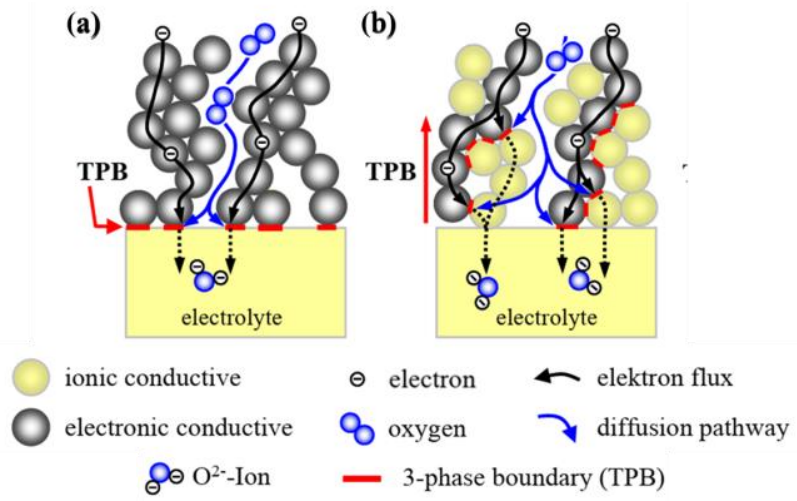

Figure 4. The triple-phase boundary (TPB) regions highlighted in red, within two cases: (**a**) where a pure electronic conductor interfaces with an electrolyte; and (**b**) within a cermet material. Reprinted with permission from Ref. [58], 2012, KIT Scientific Publishing.

As depicted in Figure 4, if the electrode is a pure electronic conductor, the migration of oxygen ions within the electrolyte towards the TPB and the movement of electrons generated at the TPB are limited to the interface between the electrolyte and the electrode. In cermet materials, which combine metal with a pure ionic conductor, an increased presence of TPB regions can be observed in comparison to materials that are solely electronic conductors. Nonetheless, certain potential TPB sites might become inactive due to either the absence of an oxygen pathway leading to the TPB zones (1) or the inability of electrons (2) to reach the current collector.

Alternatively, a two-dimensional extension of the TPB can be realized by employing mixed ionic and electronic conductors (MIEC), as depicted in Figure 5.

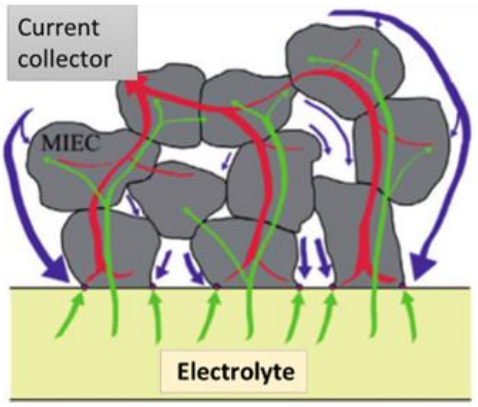

Figure 5. The flow of charge and mass within the TPB in MIEC electrode. Reprinted with permission from Ref. [59], 2011, Elsevier.

In Figure 5, the green pathway represents the movement of either holes or electrons, the red pathway signifies the migration of oxygen vacancies or O^{2-} ions, and the blue pathway indicates the movement of reactant gases or surface-adsorbed species. In this context, electrochemical reactions can take place on the surfaces of mixed ionic-electronic conductors that are in contact with gas.

As mentioned before, the functional layer is between 5 to 10 µm, where the electrochemical processes take place is often considered the "true electrode". In addition to intrinsic material properties, the focus on microstructural refinement down to the nanoscale is crucial for enhancing electrode performance under reduced temperatures. This involves the transformation of the effective feature size of the catalytic phase, transitioning from the microscale (10^{-6}) to the nanoscale (10^{-9}). Such a transition leads to a remarkable increase in electrochemical reaction sites (TPBs) by a factor of 10^9 due to the exceptionally high specific surface area. This increase has the potential to offset the exponential decrease in the activation polarization observed at the electrode as temperature decreases [55]. Furthermore, by increasing the surface-to-volume ratio, nanostructures can enhance catalytic activity and greatly improve the SOFC performance.

7.2. Oxygen Ions Conduction Mechanism

Nanomaterials such as YSZ, CGO, LSM, GDC, and LSGM are recognized as oxide-ion conductors. The fundamental characteristic enabling oxide-ion conduction is the existence of oxygen vacancies. Typically, doping involves substituting a cation of lower valence into the lattice, which also introduces oxygen vacancies to maintain overall charge balance [60]. These vacancies serve as sites for oxygen ion migration, thereby facilitating ionic conductivity. The mechanism of oxide-ion conduction in a nonstoichiometric perovskite (e.g., $Ba_4Ca_2Nb_2O_{11}$) is illustrated in Figure 6.

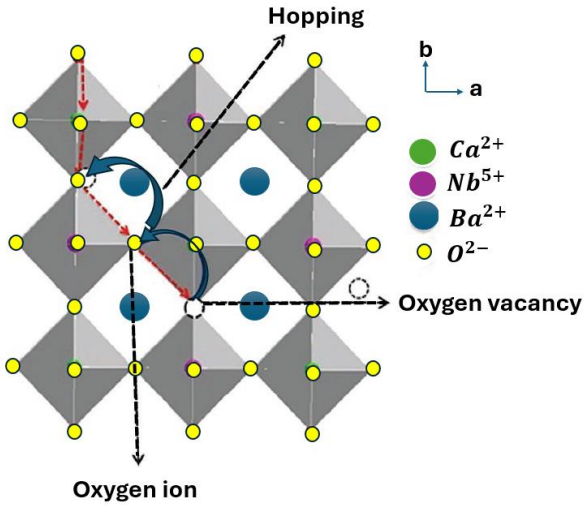

Figure 6. Oxide-ion conduction in non-stoichiometric perovskite oxide [60].

At high temperatures, due to lattice vibrations and the gradient in the chemical potential, the oxide ions migrate toward adjacent oxygen vacancies. Furthermore, the vacancy created by the displacement of an oxide ion is immediately filled by another neighboring oxide ion. This migration occurs through thermally induced hopping of oxide ions, moving from one crystal lattice position to an adjacent position, coupled with a synchronous drift aligned with the electric field. The oxygen defects determine the ionic conductivity because the ionic conductivity of a material is directly proportional to the concentration of lattice defects [61].

The value of the ionic conductivity can be determined from the concentration (n) and the mobility (μ) of the oxygen vacancies according to the following expression [62]:

$$\sigma_i = ne\mu, \tag{13}$$

where e is unit charge.

This mechanism is responsible for the transporting of oxygen ions from the cathode to the anode. At the cathode, oxygen molecules (O_2) from the air react with electrons (e^-) to produce oxygen ions ($O_2{}^-$), which then migrate through the electrolyte to the anode.

7.3. Numerical Modling

Numerous model calculations provide support for the concept that reducing particle size significantly extends the TPB length within composite electrodes and improve the SOFC characteristics. For example, WH Tanveer et al. [63] investigated simulations of thin-film anodes involving the use of high-resolution field emission scanning electron microscopy FE-SEM and high-resolution scanning transmission electron microscopy HRTEM images.

They simulate a Ni-SDC composite anode, as shown in Figure 7, like in the HRTEM image, and calculate the volume fractions of the different components of the cermet anode with the help of high-resolution FE-SEM images. The TPB density was calculated by the volume expansion method (VEM), the electrochemical reactions were based on Butler–Volmer equations, and the local charge transfer rate at the Ni-SDC anode is given by Equations (14) and (15), as follows.

$$i_{TPB} = i_0 \left[exp\left(\frac{2F}{R_0 T} \eta_{act} \right) - exp\left(-\frac{F}{R_0 T} \eta_{act} \right) \right], \tag{14}$$

$$i_0 = i_{0,TPB} l_{TPB}, \tag{15}$$

where i_0 is the exchange current density per unit length of TPB.

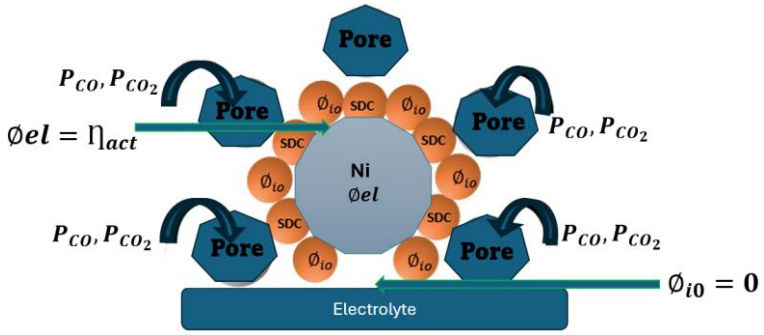

Figure 7. Schematic representation of the nanostructured Ni-SDC anode for simulation, inspired by the FE-SEM/STEM pictures [63].

The simulation results closely matched the experimental ones, especially for the upper range of intermediate-temperature SOFCs. It is noteworthy that this served as the inaugural example of reconstructing and simulating porous electrodes at the nanometer scale using direct 2D imaging techniques. The resulting structures demonstrated exceptional performance, exceeding results previously reported in the literature for fuel cells operating under CO_2-reduced electrolytic integrated water conversion (IWC) fuel conditions. The exceptional performance was attributed to several factors such as the high density of ternary phase boundaries, the systematically organized structure that prevents agglomeration, reduced tortuosity, and the enhanced communication of fuel gases within the nanostructured cermet anode.

Electrode materials typically consist of doped perovskite for the cathode and Ni oxide cermet for the anode. However, up to this point, there has not been much research on precisely controlling the nano size of the electrode catalyst due to the high operating temperatures. Nevertheless, there is growing enthusiasm for exploring nano size-controlled materials now, given the potential for lower-temperature operation, which could significantly enhance the power output and the durability of SOFCs.

In addition, minimization of electrolyte thickness to reduce the oxygen ion diffusion path length is one of the most intuitive strategies to reduce ohmic polarization losses, thus providing desirable electrolyte area-specific resistance ASRs at reduced temperature [55]. This approach recognizes that shorter diffusion distances can significantly enhance overall efficiency. However, it is challenging to fabricate microcrack- or pore-free thin ceramic electrolytes below 1 μm uniform thickness. Achieving such precision at the nanoscale level requires innovative techniques and materials.

Thus, various nanotechnology-based thin-film deposition methods have been employed to establish nanoscale electrolytes. These techniques leverage the unique properties of nanomaterials to create thin and uniform electrolyte layers. In the next section, we will delve into the experimental details regarding the utilization of nanomaterials for the electrolyte, anode, and cathode of the SOFC.

8. Poisoning and Contamination of Ni-Based Anode for SOFC

Anode degradation in SOFCs poses a significant challenge, often resulting from unfavorable reactions and the poisoning of Ni-based anode materials by sulfur or carbon species. Sulfur commonly manifests as H_2S. Despite the existence of desulfurization methods for fuels before their introduction into cell systems [64], the residual concentrations of H_2S typically fluctuate between 0.1 and 15 ppm [65–67]. These concentrations have been demonstrated to significantly impact the performance and longevity of the cells. Hence, effectively utilizing commercially available fuels in SOFC power generators poses a significant challenge, which critically depends on the effective control of degradation parameters at the anode electrode. For the formation and deposition of carbon, it results from internal reforming and oxidation reactions of hydrocarbons (H/Cs) in SOFCs. Various

factors play a significant role in determining its occurrence, and the characteristics of the catalyst/anode stand out as particularly crucial [68].

To address these challenges, global research endeavors primarily concentrate on advancing anode materials that are both efficient and resilient against carbon deposition and sulfur poisoning in the event of desulphurization system malfunctions [69,70], all while upholding superior electronic conductivity and electrocatalytic performance.

Many alternative anode materials exhibit improved sulfur tolerance, such as $CuFeS_4$, Cu–CeO_2/YSZ, $La_{0.4}Sr_{0.6}TiO_3$, $La_{0.75}Sr_{0\cdot25}Cr_{1-x}MnxO_3$, $Sr_2Mg_{1-x}Mn_xMoO_{6-\delta}$ and $Ce_{0.9}Sr_{0.1}Cr_{0.5}Fe_{0.5}O_{3-1}$, $La_{0\cdot7}Sr_{0.3}VO_3$, $Gd_2Ti_2O_7$, and other formulations [69,71,72]. Vincent et al. [73] conducted research on anode-based $La_{0.4}Sr_{0.6}TiO_{3-\delta}$/YSZ, demonstrating its stability in an H_2S environment, even at very high concentrations, where conventional Ni-based anodes typically fail. Specifically, the investigated cell exhibited a notable enhancement in power density, increasing from 2 $mWcm^{-2}$ when fueled by pure CH_4 to over 450 $mWcm^{-2}$ when CH_4 contained 20 vol.% H_2S.

For Ru and Rh, it has been proposed that the formation of carbon deposits may not occur significantly due to the limited solubility of carbon in these metals [74,75]. However, their high cost makes them prohibitively expensive for use in SOFC applications. Other research [76–79] has highlighted that Sn/Ni surface alloy exhibits greater tolerance to carbon compared to pure Ni when exposed to conditions involving steam reforming of methane, propane, and isooctane at moderate steam-to-carbon ratios. This alloy also demonstrates resilience under direct electrochemical oxidation of methane and isooctane. Additionally, Cu/YSZ anodes have shown stability in oxidizing hydrocarbons, and Cu supported on ceria (such as Cu-CeO_2/YSZ anodes) has been repeatedly cited as a stable electrooxidation catalyst under internal reforming conditions [70,80–83].

9. Experimental Details on Nanostructured Materials for SOFC

The integration of nanostructured materials into the components of SOFCs has revolutionized the field of energy conversion and storage [84]. These nanostructured components, including electrolytes, anodes, and cathodes, offer enhanced properties and improved performance, making them pivotal in advancing the efficiency and applicability of SOFC technology [85]. The fabrication method of these nanostructured materials is a crucial aspect of their successful implementation, as it governs their structural characteristics, electrochemical behavior, and overall functionality within the fuel cell system [86]. In this section, we delve into the diverse synthesis approaches that support the creation of nanostructured materials for SOFC components. By exploring approaches spanning from sol–gel techniques to atomic layer deposition and beyond, we explore how these approaches enable precise control over the material's nanostructure, grain size, and surface area. This subsection seeks to shed light on the intricate relationships between synthesis methods and the resulting nanostructured materials, emphasizing their profound impact on the overall performance and potential applications of SOFCs.

9.1. Electrolyte Preparation and Its Impact on Ionic Conductivity

The pursuit of high efficiency and enhanced performance in SOFCs has prompted a keen focus on the development of advanced electrolyte materials [87]. As a key component of SOFCs, the electrolyte facilitates oxygen ion mobility and maintains ionic conductivity at high temperatures [88]. These synthesis methods intricately shapes the ionic transport capabilities of the electrolytes, impacting the overall efficiency and reliability of the fuel cell system [89]. This section explores the various electrolyte preparation methods and their profound impact on ionic conductivity in SOFCs. By examining various techniques such as sol–gel, atomic layer deposition, and pulsed laser deposition, we aim to provide an insightful overview of how these methods contribute to the quest for improved SOFC performance. In the context of SOFCs, the sol–gel method provides a means to synthesize electrolyte materials with controlled nanostructures. By adjusting parameters such as precursor type, solvent, pH, and drying conditions, researchers can tailor the properties

of the resulting electrolyte material to meet specific SOFC requirements. For example, using a simple sol–gel technique, Xu et al. [88] created a fast ion-conducting electrolyte based on a doped $LaAlO_3$ with an amorphous surface layer (LSAZ). The as-prepared SOFC electrolyte material exhibits a superior conductivity of 0.319 S cm^{-1} at 550 °C, and it is used in a solid oxide fuel cell that demonstrates a remarkable performance of 1296 mW cm^{-2} at 550 °C, which is 300 times higher than a solid oxide fuel cell with the LSAZ being densified at 1400 °C for 10 h. Furthermore, Chen et al. [90] assessed the ion conduction mechanism for the $Ce_{0.9}Gd_{0.1}O_{2-\delta}$ (GDC) electrolyte based on a nanocrystalline structure fabricated through the sol–gel method. Their study uncovered that ionic conduction at interfaces between particles is the dominant conduction mechanism of the GDC electrolyte with nanocrystalline structure. The resulting device demonstrated an extremely high ionic conductivity of 0.37 S·cm^{-1} and exhibited an impressive performance of 591.8 mWcm^{-2} at 550 °C, marking a noteworthy improvement of approximately 3.5 times compared to the cell with the GDC electrolyte densified at 1550 °C. Likewise, Shah and coworkers [91] manufactured a GDC electrolyte through a chemical co-precipitation method, utilizing Na_2CO_3 as the precipitating agent. It is known that co-precipitation involves the simultaneous precipitation of cations to form nanoparticles, facilitating precise control over particle size [92]. Figure 8 shows the process of preparing the Mg-Doped $Sr_{0.5}Pr_{0.5}Fe_{0.2}Mg_{0.2}Ti_{0.6}O_{3-\delta}$ nanostructured material.

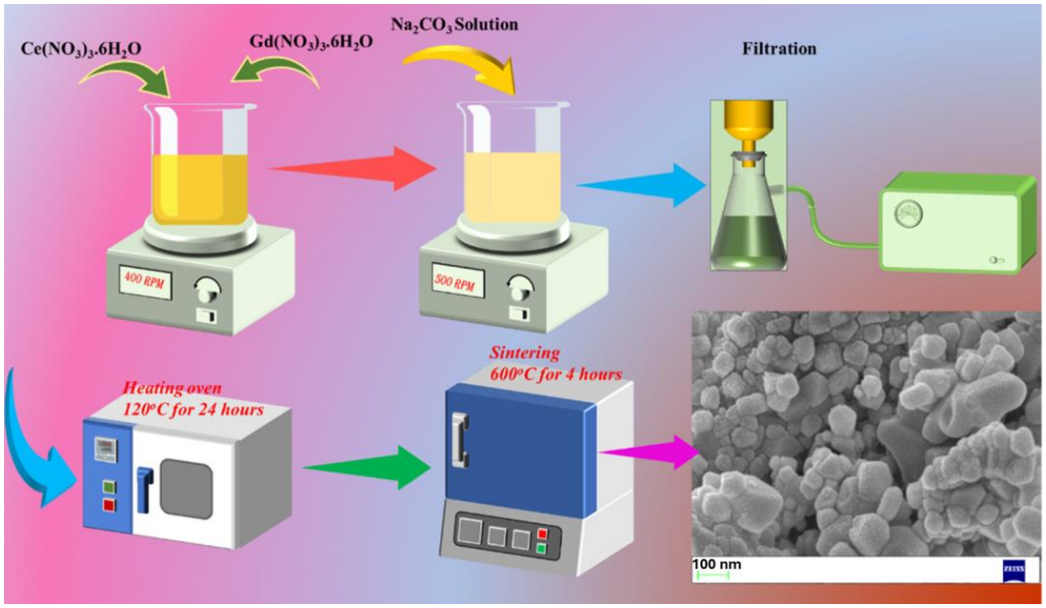

Figure 8. Schematic illustration depicting the synthesis procedure of GDC with its morphology. Reprinted with permission from Ref. [91], 2023, Elsevier.

Their investigation unveiled that the synthesized GDC electrolyte exhibits impressive fuel cell performance, reaching 569 mW/cm^2, coupled with a high ionic conductivity of 0.1 S/cm at a relatively low temperature of 450 °C. Furthermore, when integrated into a fuel cell device, the synthesized GDC demonstrated exceptional stability, maintaining its operation for 150 h at a high current density of 110 mA/cm^2, all while operating at 450 °C. They indicated that the high ionic conductivity is attributed to surface or grain boundary conduction. Rauf et al. [93] explored the impact of Mg doping in the $Sr_{0.5}Pr_{0.5}Fe_{0.4}Ti_{0.6}O_{3-\delta}$ perovskite to synthesize the SPFM$g_{0.2}$T electrolyte material using a hydrothermal technique assisted by the co-precipitation method. To prepare the optimal electrolyte material, precursors such as $Sr(NO_3)_2$, $Pr(NO_3)_{2\cdot6}H_2O$, $Mg(NO_3)_{2\cdot6}H_2O$, $Fe(NO_3)_{3\cdot9}H_2O$, and TiO_2 were used. The acquired $Sr_{0.5}Pr_{0.5}Fe_{0.2}Mg_{0.2}Ti_{0.6}O_{3-\delta}$ (SPFM$g_{0.2}$T) has established its position as an ideal electrolyte material, presenting both a notable ionic conductivity of 0.133 S.cm^{-1} and an impressive fuel cell performance of 0.83 W.cm^{-2} at 520 °C. Their investigation

revealed that Mg doping enhances ionic conductivity and fuel cell performance, resulting in elevated open-circuit voltages (OCVs). The study sheds light on the structure of the material's core–shell which includes a semiconducting core and an ionic superconducting surface layer. Moreover, it proposes that the interplay between electrons and oxide ions (oxygen vacancies) within this core–shell-based heterostructure introduces a novel scientific mechanism for superionic conduction in the SPFM$g_{0.2}$T electrolyte, especially in low-temperature solid oxide fuel cells (LT-SOFCs), where the interface/surface assumes a pivotal role. Similarly, based on the solid-state reaction method, Akbar et al. [94] developed a nanoscale heterostructure electrolyte based on layered $NaCo_{0.5}Fe_{0.5}O_2$ (NCF) and fluorite CeO_2, in which Na_2CO_3 was used as precipitating agent. The introduction of a layered semiconductor NCF into the fluorite structure ionic oxide CeO_2 resulted in a significant increase in ionic conductivity and a strong chemical stability of the electrolytic material. Their discovery revealed that the NCF-CeO_2 heterostructure forms extensive hetero-interfaces and accumulates oxygen vacancies, resulting in enhanced ionic conductivity. The resulting device showed strong chemical stability along with a high-power density (PPD of 1010 mW cm^{-2} at 550 °C with 160 h stability).

In another study, Li et al. [95] successfully fabricated an electrolyte component for SOFC by developing a composite of YSZ and $Ce_{0.8}Sm_{0.2}O_{1.9}$ (SDC) materials using a thermal inkjet printing method that utilized inks with a high solid content. The as-prepared cell, measuring 1.5 µm in thickness, reached a peak power density of 860 mW cm^{-2} when operating at 800 °C. Similarly, Shim et al. [96] developed ultrathin YSZ electrolyte films, precisely 60 nm thick, exhibiting an optimal composition ratio (7–8% Y_2O_3) when deposited on Si_3N_4 substrates via the atomic layer deposition (ALD) method. Their study revealed that the improvement in performance resulted from an increased exchange current density at the interface between the electrode and electrolyte. This single cell achieved an open circuit voltage (OCV) ranging from 1.02 to 1.10 V and power densities of 28 to 270 mW/cm^2 across the temperature range of 265 °C to 350 °C.

9.2. Anode Preparation and Its Effect on Electrocatalytic Activity

The unique structural features of nanostructured materials, including high surface area, finely tuned porosity, and exceptional conductivity, have revolutionized the landscape of anode design [97]. These materials, often composed of ceria-based oxides, perovskite oxides [98], or composite structures [99], have enabled performance breakthroughs, providing both higher power output and superior operational flexibility. Anode preparation, a multidimensional process, encompasses various techniques, including sol–gel methods, co-precipitation, and sophisticated deposition processes, each playing its unique note in crafting the ideal anode structure. The catalyst is a pivotal actor as it engages in intricate redox reactions, the very essence of energy conversion within SOFCs. The catalyst loading, a delicate balance between sufficiency and excess, influences the reactivity of the anode electrode. Morphological nuances, spanning from nanowires and nanoparticles to thin films, alter the landscape of catalytic surfaces. The precise composition, often a blend of elements carefully chosen for their catalytic properties, orchestrates the performance of nanostructured anodes. In the advanced stages of anode development, Yildirim and his colleagues developed and optimized nanostructured anode material prepared using an infiltration method (Figure 9), in which nickel was infiltrated into the porous YSZ backbone as a catalyst [100]. The fuel cell device using this anode exhibited a significantly enhanced power output (~0.4 W/cm^2 at 800 °C), which is more than double the power (0.174 W/cm^2) measured from the reference cell under the same test conditions. Their study conclusively illustrated that nickel catalyst infiltration is an exceptionally effective approach for enhancing cell performance. This strategy results in an augmented number of electrochemical reaction zones within the anode electrode, thanks to the formation of nanostructured nickel catalysts around the primary YSZ phase.

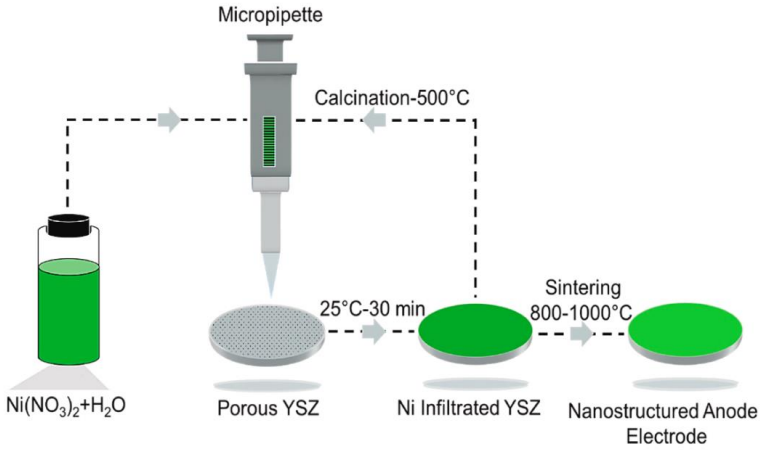

Figure 9. A schematic illustration of the stages used to prepare a nanostructured anode through infiltration. Reprinted with permission from Ref. [100], 2023, Elsevier.

In a similar context, M. Singh et al. [101] pioneered the development of a novel NiO-GDC nanowire anode using the vapor–liquid–solid (VLS) method. The study offers valuable insights into the reorganization of NiO-GDC particles, leading to the creation of the nanowires from the pristine NiO-GDC powder. Additionally, the analysis of temperature-dependent electrical conductivity indicates that nanowires synthesized at 1400 °C display substantially enhanced conductivity, a result of improved charge-carrier transport, as evidenced by their remarkably low activation energies. Also, the cell demonstrates a peak power density of approximately 178 mW.cm^{-2} at 800 °C.

Furthermore, to enhance the conductivity and catalytic performance of nanostructured anode materials, Somacescu et al. [102] developed an advanced hydrothermal synthesis method to create bimodal mesoporous NiO/$CeO_{2-\delta}$YSZ anode, incorporating CTAB and TPA as templates. Their research findings confirm the effective dispersion of Ni and Ce within the YSZ lattice in the designed anode material. It was observed that an increase in the percentage of Ce^{3+} and the formation of NiO facilitated improvements in both electrical conductivity and catalytic activity. Moreover, this specific anode displays significantly enhanced resistance to carbon deposition when applied in the catalytic partial oxidation of methane. Likewise, Shi et al. created a promising anode by utilizing a finger-like porous YSZ as the anode substrate and impregnating it with $Ni_{0.08}Co_{0.02}Ce_{0.9}O_{2-\delta}$@$Ni_{0.8}Co_{0.2}O$ as the innovative catalyst, fabricated through the phase conversion-combined tape-casting technique, as shown in Figure 10 [103]. The as-synthesized anode demonstrates remarkable mechanical strength, outstanding catalytic activity, and stability in methane conversion reactions. These qualities can be attributed to the exsolved alloy nanoparticles, the presence of active oxygen species on the reduced $Ni_{0.08}Co_{0.02}Ce_{0.9}O_{2-\delta}$ catalyst, and the enhanced methane transport facilitated by the special open-pore microstructure of the anode substrate, whereas the significance of advancing highly efficient anode materials as alternatives to Ni-based anodes is steadily increasing in importance for the commercialization of SOFCs. Zhang and their colleagues synthesized a series of Ni-free anode materials decorated with metal nanoparticles through the in situ reduction of Fe-doped $Sr_2CoMo_{1-x}Fe_xO_{6-\delta}$ (x = 0, 0.05, 0.1) double perovskite oxides under reducing conditions at 850 °C [104]. The $SCMF_{0.05}$-supported cell exhibits outstanding performance, achieving peak power densities of 992.9 mW cm^{-2} in H_2 and 652.3 mW cm^{-2} in CH_4 at 850 °C. Furthermore, it displays exceptional stability, operating reliably for approximately 50 h at 700 °C. Their research findings highlight that the in situ exsolution of multiple-twinned Co–Fe nanoparticles leads to a substantial improvement in anode performance and coking resistance. Similarly, Li et al. [105] designed and developed two new anodes by employing $La_{0.6}Sr_{0.4}Ni_{0.2}Mn_{0.2}Fe_{0.6}O_{3-\delta}$ (LSNMF) and $La_{0.6}Sr_{0.4}Co_{0.2}Mn_{0.2}Fe_{0.6}O_{3-\delta}$ (LSCMF) perovskite oxides as precursor materials. These were utilized for the in situ fabrication of RP-structured perovskite oxide ($La_{1.2}Sr_{0.8}Mn_{0.4}Fe_{0.6}O_{4-\delta}$, RP-LSMF), along with

Fe_3Co_2/Fe_3Ni_2 nanoparticles. This innovative approach was geared towards enhancing the performance of SOFCs operating with H_2S-containing fuels. Exceptional device performance was confirmed through validation using an electrolyte-supported SOFC equipped with a Fe_3Co_2/RP-LSMF anode, achieving impressive power densities of 632 $mWcm^{-2}$ and 566 $mWcm^{-2}$ when operating with H_2 and a mixture of 200 ppm H_2S–H_2 at 800 °C, respectively. They discovered that the RP-LSMF anode decorated with CoFe alloy exhibited significantly greater electrocatalytic activity and sulfur tolerance. This improvement stems from the presence of a larger amount of dissolved alloy nanoparticles on the surface and a more pronounced coupling effect with the RP perovskite substrate compared to the RP perovskite-based anode modified with NiFe alloy. In a parallel study, Choolaei and colleagues [106] synthesized nanocrystalline powders of Co_{1-x}-Zn_x-$Gd_{0.1}Ce_{0.9}O_{1.95}$ (with x values of 0.50 and 0.65) through a co-precipitation method. They then utilized these materials as components in a nickel-free composite for SOFC anodes. Their investigation revealed that the introduction of Zn into the Co-based anode composite led to a remarkable enhancement in the cell's performance at low and intermediate temperatures, surpassing that of the Co-GDC-based cell by more than fivefold. This enhancement was accompanied by a noticeable increase in the cell's open-circuit voltage (OCV), which reached approximately 0.91 V at 650 °C.

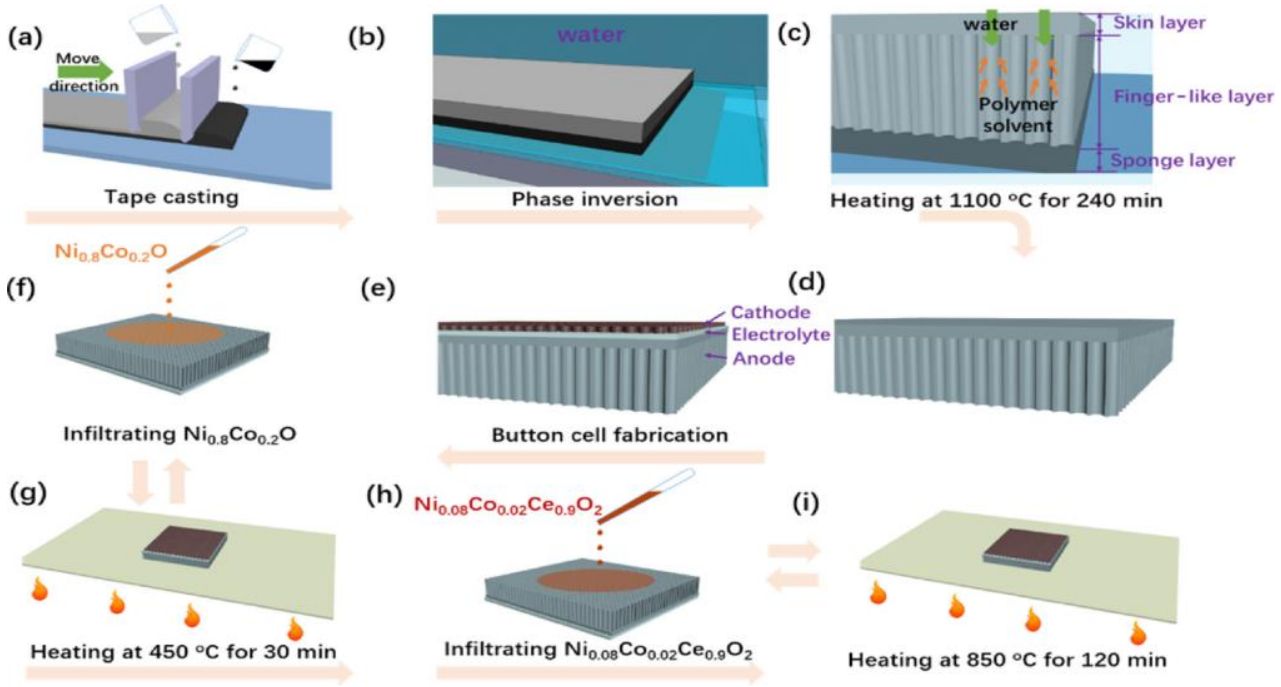

Figure 10. Schematic diagram of anode-equipped button cell preparation process. (**a**) tape-casting process, (**b**,**c**) phase inversion process, (**d**) microstructure of the anode substrate, (**e**) microstructure of the button cell, (**f**) infiltrating $Ni_{0.8}Co_{0.2}O$ to the anode, (**g**) heating process, (**h**) infiltrating $Ni_{0.08}Co_{0.02}Ce_{0.9}O_2$ to the anode, and (**i**) firing process to complete cell fabrication. Reprinted with permission from Ref. [103], 2021, American Chemical Society.

9.3. Cathode Preparation and Its Role in Enhancing Oxygen Reduction Kinetics

Cathode preparation is another crucial aspect of SOFC development, impacting the kinetics of oxygen reduction reactions and, consequently, the overall performance of these clean energy devices [107]. Ongoing research and innovation in cathode preparation techniques promise to further enhance the efficiency and viability of SOFCs, making them a compelling solution for a sustainable energy future [108]. Hence, the choice of synthesis method depends on the desired properties and performance characteristics of the resulting nanostructured cathode electrode material. As an illustration, Li et al. [109] utilized soluble salts as the source of metal ions and polyacrylonitrile (PAN) as the poly-

mer matrix in the fabrication of a cathode material displaying a fibrous morphology, specifically $La_{1.2}Sr_{0.8}CoO_{4\pm\delta}$, through the electrostatic spinning process. Their study revealed that in contrast to conventional cathode materials featuring a plain granular structure, the $La_{1.2}Sr_{0.8}CoO_{4\pm\delta}$ fibril exhibits a superior microscopic morphology and demonstrates more advanced electrochemical properties. Certainly, when operating at 800 °C, the $La_{1.2}Sr_{0.8}CoO_{4\pm\delta}$ fibrous cathode exhibits outstanding performance, featuring an impressively low polarization resistance of 0.043 Ω.cm^2 and achieving a peak power output of 716 mW.cm^{-2}. This confirms its ability to demonstrate swift electrode kinetics during the O^2 reduction reaction. Similarly, Ma et al. [107] innovatively developed a cathode material consisting of nanoparticles of magnesium-doped manganese–chromium spinel oxide. In this study, the impregnation method is utilized to produce uniformly dispersed nanoparticles of magnesium-doped manganese–chromium spinel oxide, which are then integrated into a network within the $Gd_{0.1}Ce_{0.9}O_{1.95}$ (GDC) skeleton for use as SOFC cathodes. Their investigation revealed that the introduction of Mg through doping optimizes the electronic structure of manganese-chromium spinel oxide, increases the concentration of oxygen vacancies, and significantly enhances both electrical conductivity and catalytic activity in the context of the ORR. The as-prepared Mg-doped Mn–Cr spinel cathode demonstrates exceptional performance, featuring an area-specific polarization resistance of 0.33 Ω.cm^2 and a maximum power density of 976 mW.cm^{-2} at 800 °C. In an interesting study conducted by Zhang et al. [110], they achieved successful deposition of a nanostructured cathode composed of $La_{0.6}Sr_{0.4}Co_{0.2}Fe_{0.8}O_{3-\delta}$ (LSCF) using vacuum cold spray (VCS). To attain this, the LSCF spray powders were precisely manufactured through the Pechini method and subsequently underwent a controlled low-temperature annealing process, effectively preventing both strontium (Sr) surface segregation and particle coarsening. Their findings revealed that the VCS-sprayed nanostructured LSCF cathode maintained stable performance owing to the consistent microstructure and the controlled presence of surface-segregated Sr throughout cell operation. They found that optimizing the microstructure of the LSCF cathode offers a straightforward path to significantly enhance the performance of the oxygen reduction reaction. Fuel cell device using this nanostructured cathode showed remarkable peak power densities of >1 W.cm^{-2} at 600 °C and >0.2 W.cm^{-2} at 450 °C, along with good stability for ~500 h. Moreover, Farhan and colleagues utilized the sol–gel process to fabricate a series of multi-phase cathodes denoted as $Fe_{0.25-x}Mn_xCe_{0.75}O_{2-\delta}$ (with x values of 0.0, 0.02, 0.04, and 0.06). The precursors employed in this procedure consisted of Fe $(NO_3)_{3\cdot9}H_2O$, Mn $(NO_3)_{2\cdot4}H_2O$, and Ce $(NO_3)_{3\cdot6}H_2O$ [111]. They found that the inclusion of Mn^{3+} and Fe^{3+} ions into CeO^2 created additional oxygen vacancies and significantly enhanced the ceria catalytic activity and oxygen kinetics for redox-based reactions. The addition of suitable Mn content had a profound impact on the electrical conductivity of the prepared samples. The $Fe_{0.25-x}Mn_xCe_{0.75}O_{2-\delta}$ cathode cell exhibits outstanding performance, achieving a peak power density of 335 mW.cm^{-2} at 550 °C, along with an open-circuit voltage (OCV) reaching a value of ~0.98 V. In another study by Tang et al. [112], a composite cathode material was synthesized by infiltrating nanostructured $LaNi_{0.6}Fe_{0.4}O_{3-\delta}$ (LNF) into $La_2NiO_{3-\delta}$ (LNO). The starting materials used for powder synthesis comprised $Ni(NO_3)_{2\cdot6}H_2O$, $BaCO_3$, $Zr(NO_3)_{4\cdot5}H_2O$, $Ce(NO_3)_{3\cdot6}H_2O$, $Y(NO_3)_{3\cdot6}H_2O$, La_2O_3, and $Fe(NO_3)_{3\cdot9}H_2O$. The extensive adoption of this approach, which involves the use of composite infiltration solutions, emphasizes the remarkable versatility of the technique. The study they presented, which involved cells with LNO cathodes and LNF-infiltrated LNO cathodes, demonstrates that infiltrated cathode materials can notably enhance the electrochemical properties and improve the kinetics of ORR. Utilizing the LNF-infiltrated LNO cathode, the fuel cell device demonstrated remarkable performance, achieving the highest power density of 969 mW.cm^{-2} and recording the lowest polarization resistance, measuring 0.027 Ω.cm^2 at 700 °C.

Table 3 summarizes recent reports on the fabrication of nanostructured materials for SOFC applications, along with the performance data of several representative single-component SOFCs.

Table 3. Recent works on nanostructured materials for SOFC applications.

SOFC-Components	Synthesis Method	Ionic Conductivity (S/cm)	Power density (mW/cm^2)	Operating Temperature (°C)	Reference
Electrolyte					
LSAZ	Sol–gel method	0.319	1296	550	[85]
GDC	Sol–gel	0.37	592	550	[87]
GDC	Chemical coprecipitation method	0.1	569	450	[88]
SPFMg$_{0.2}$T	Hydrothermal assisted by the coprecipitation method	0.133	830	520	[90]
NCF-CeO_2	Solid-state reaction method	0.16	1010	550	[91]
YSZ	Thermal inkjet printing method	No data	860	800	[92]
YSZ	Atomic layer deposition (ALD)	No data	28–270	265–350	[93]
Anode					
Ni-YSZ	Infiltration approach	No data	400	800	[97]
NiO-GDC	Vapor–liquid–solid (VLS)	No data	178	800	[98]
NC-$CeO_{2\ x}$@NC@YSZ	Phase conversion-combined tape-casting	No data	730	800	[100]
Fe-doping Sr_2CoMo_1 $xFexO_{6-\delta}$	In situ reduction route	No data	993	850	[101]
Fe_3Co_2/RP-LSMF	Sol–gel/in situ fabrication	No data	632–566	800	[102]
Co-GD & $CoZn_{50}$-GDC	Co-precipitation method	No data	10 & 77	750	[103]
Cathode					
LSC128	Electrostatic spinning	No data	716	800	[106]
Mg-doped Mn–Cr spinel	Impregnation method	3.19	976	800	[104]
LSCF	Vacuum cold spray (VCS)	No data	1040	600	[107]
FMDC4	Sol–gel method	0.89	335	550	[108]
Infiltrated LNF-LNO	Infiltration method	No data	969	700	[109]

10. Challenges and Obstacles

The integration of nanomaterials into SOFCs presents promising opportunities to significantly improve their performance. Yet, this pursuit is fraught with numerous challenges and obstacles that researchers must overcome. This review thoroughly examines the major obstacles encountered during the fabrication of nanomaterials and nanostructures for SOFCs, highlighting innovative strategies pursued to overcome them.

However, overcoming various challenges is essential to fully capitalize on their potential in SOFC applications. It is challenging to develop processing techniques for nanostructured materials that are both scalable and reproducible, to control microstructure and morphology of nanostructured materials, and to address stability and durability concerns. As a result of the fabrication process and testing environment, single-component SOFCs may require more engineering efforts relating to nanostructured materials design, device assembly, and facility optimization in order to improve stability and facilitating long-term testing in future endeavors, further developing this technology. Moreover, the compatibility of nanostructured materials with other components and materials within the SOFC system must be carefully considered. So, the future outlook for nanostructured materials in SOFC applications is bright despite these challenges. Ongoing research efforts focus on developing novel synthesis methods to tailor the properties of nanostructured materials, exploring advanced characterization techniques for a comprehensive understanding of their behavior, and integrating nanostructured materials into multifunctional components to improve overall SOFC performance.

Scalability and cost-efficiency is yet another challenge. Many promising nanomaterial fabrication methods are currently expensive and not easily scalable. Achieving cost-effective large-scale production of SOFC components with nanomaterials remains a significant obstacle for commercialization.

Accurately characterizing nanomaterials and nanostructures within the harsh operating conditions of SOFCs is a significant characterization challenge. Developing advanced analytical techniques that provide real-time information about nanomaterial behavior under operational conditions is crucial.

Ensuring the durability and reliability of SOFCs with nanomaterials is also a critical challenge. While nanomaterials have the potential to enhance performance, they can introduce new failure modes, and reliability concerns that must be addressed.

Finally, environmental and safety concerns must be carefully considered. As with any emerging technology, the potential release of nanoparticles during fabrication, operation, or disposal could have adverse effects.

11. Conclusions

Advances in nanostructured material applications for SOFC, particularly in electrode materials, electrolytes, and interfacial interactions, have shown great potential in addressing the growing challenges associated with determining overall cell performance. Enhanced nanostructure materials hold significant promise for advancing SOFCs technology. Their unique properties, such as high surface area, improved conductivity, and enhanced catalytic activity, offer the potential to overcome many challenges facing SOFCs, including lower operating temperatures, increased durability, and higher efficiency. Taking advantage of the unique properties of nanostructured materials and integrating them with innovative technologies, we can advance the development of sustainable and efficient SOFC applications, ultimately ensuring global access to clean energy. This work has highlighted the significant progress made by nanostructured materials in the field of SOFC, with a particular focus on the fabrication of their components. In addition, this review has also highlighted the many different techniques and routes available to fabricate nanostructured materials and pat-terns for SOFC applications, with each method offering its own merits and drawbacks in terms of microstructure and quality. Despite the remarkable progress in the fabrication and optimizing nanostructured materials with high ionic conductivity and electronic structures, several challenges and perspectives for nanomaterial design and synthesis need to be taken into account to achieve realistic high energy density, greater electrocatalytic activity, and future practical applications. Further studies are still needed for different types of nanomaterials with high efficiency and enhanced catalytic activity, and the durability of these nanostructured materials is an ongoing task for the development of the next-generation SOFCs with high energy performance.

Continued research and development in this area are crucial for realizing the full potential of SOFCs as a clean and efficient energy solution for the future.

Author Contributions: Conceptualization, E.C. and D.Z.; methodology, H.H.; validation, E.C. and D.Z.; writing—original draft preparation, E.C., D.Z. and H.H.; writing—review and editing, H.H., M.A. and A.R.; visualization, H.H.; supervision, E.C. and D.Z.; funding acquisition, E.C. and D.Z. All authors have read and agreed to the published version of the manuscript.

Funding: This study was carried out within the MOST—Sustainable Mobility National Research Center and received funding from the European Union Next-Generation EU (PIANO NAZIONALE DI RIPRESA E RESILIENZA (PNRR)—MISSIONE 4 COMPONENTE 2, INVESTIMENTO 1.4—D.D. 1033 17/06/2022, CN00000023), Spoke 5 "Light Vehicle and Active Mobility". This manuscript reflects only the authors' views and opinions; neither the European Union nor the European Commission can be considered responsible for them. Also, we are thankful to MUR PON DM 1061 for funding this study.

Data Availability Statement: The original contributions presented in the study are included in the article, further inquiries can be directed to the corresponding authors.

Acknowledgments: Artificial Intelligence software, namely, ChatGPT 3.5, was used to revise the English language of the manuscript.

Conflicts of Interest: The authors declare that have no conflicts of interest/competing interests.

References

1. Sreedhar, I.; Agarwal, B.; Goyal, P.; Singh, S.A. Recent advances in material and performance aspects of solid oxide fuel cells. *J. Electroanal. Chem.* **2019**, *848*, 113315. [CrossRef]
2. Owusu, P.A.; Asumadu-Sarkodie, S. A review of renewable energy sources, sustainability issues and climate change mitigation. *Cogent Eng.* **2016**, *3*, 1167990. [CrossRef]
3. Singh, M.; Zappa, D.; Comini, E. Solid oxide fuel cell: Decade of progress, future perspectives and challenges. *Int. J. Hydrogen Energy* **2021**, *46*, 27643–27674. [CrossRef]
4. Lyu, Y.; Xie, J.; Wang, D.; Wang, J. Review of cell performance in solid oxide fuel cells. *J. Mater. Sci.* **2020**, *55*, 7184–7207. [CrossRef]
5. Kuterbekov, K.A.; Nikonov, A.V.; Bekmyrza, K.Z.; Pavzderin, N.B.; Kabyshev, A.M.; Kubenova, M.M.; Kabdrakhimova, G.D.; Aidarbekov, N. Classification of solid oxide fuel cells. *Nanomaterials* **2022**, *12*, 1059. [CrossRef] [PubMed]
6. Choolaei, M.; Vostakola, M.F.; Horri, B.A. Recent Advances and Challenges in Thin-Film Fabrication Techniques for Low-Temperature Solid Oxide Fuel Cells. *Crystals* **2023**, *13*, 1008. [CrossRef]
7. Pikalova, E.Y.; Kalinina, E.G. Solid oxide fuel cells based on ceramic membranes with mixed conductivity: Improving efficiency. *Russ. Chem. Rev.* **2021**, *90*, 703. [CrossRef]
8. Zakaria, Z.; Awang Mat, Z.; Abu Hassan, S.H.; Boon Kar, Y. A review of solid oxide fuel cell component fabrication methods toward lowering temperature. *Int. J. Energy Res.* **2020**, *44*, 594–611. [CrossRef]
9. Matthew, O.; Nieh, S. Effects of ORC Working Fluids on Combined Cycle Integrated with SOFC and ORC for Stationary Power Generation. *Energy Power Eng.* **2019**, *11*, 167–185. [CrossRef]
10. Ahmadi, M.H.; Sadaghiani, M.S.; Pourfayaz, F.; Ghazvini, M.; Mahian, O.; Mehrpooya, M.; Wongwises, S. Energy and exergy analyses of a solid oxide fuel cell-gas turbine-organic rankine cycle power plant with liquefied natural gas as heat sink. *Entropy* **2018**, *20*, 484. [CrossRef]
11. Bossel, U. Rapid startup SOFC modules. *Energy Procedia* **2012**, *28*, 48–56. [CrossRef]
12. Kariya, T.; Tanaka, H.; Hirono, T.; Kuse, T.; Yanagimoto, K.; Uchiyama, K.; Henmi, M.; Hirose, M.; Kimura, I.; Suu, K. Development of a novel cell structure for low-temperature SOFC using porous stainless steel support combined with hydrogen permeable Pd layer and thin film proton conductor. *J. Alloys Compd.* **2016**, *654*, 171–175. [CrossRef]
13. Rafique, M.; Nawaz, H.; Shahid Rafique, M.; Bilal Tahir, M.; Nabi, G.; Khalid, N. Material and method selection for efficient solid oxide fuel cell anode: Recent advancements and reviews. *Int. J. Energy Res.* **2019**, *43*, 2423–2446. [CrossRef]
14. Kilner, J.A.; Burriel, M. Materials for intermediate-temperature solid-oxide fuel cells. *Annu. Rev. Mater. Res.* **2014**, *44*, 365–393. [CrossRef]
15. Bove, R. Solid oxide fuel cells: Principles, designs and state-of-the-art in industries. In *Recent Trends in Fuel Cell Science and Technology*; Springer: New York, NY, USA, 2007; pp. 267–285.
16. Mah, J.C.; Muchtar, A.; Somalu, M.R.; Ghazali, M.J. Metallic interconnects for solid oxide fuel cell: A review on protective coating and deposition techniques. *Int. J. Hydrogen Energy* **2017**, *42*, 9219–9229. [CrossRef]
17. Yatoo, M.A.; Habib, F.; Malik, A.H.; Qazi, M.J.; Ahmad, S.; Ganayee, M.A.; Ahmad, Z. Solid-oxide fuel cells: A critical review of materials for cell components. *MRS Commun.* **2023**, *13*, 378–384. [CrossRef]
18. Choi, S.; Sengodan, S.; Park, S.; Ju, Y.-W.; Kim, J.; Hyodo, J.; Jeong, H.Y.; Ishihara, T.; Shin, J.; Kim, G. A robust symmetrical electrode with layered perovskite structure for direct hydrocarbon solid oxide fuel cells: $PrBa_{0.8}Ca_{0.2}Mn_2O_{5+\delta}$. *J. Mater. Chem. A* **2016**, *4*, 1747–1753. [CrossRef]
19. Kan, W.H.; Samson, A.J.; Thangadurai, V. Trends in electrode development for next generation solid oxide fuel cells. *J. Mater. Chem. A* **2016**, *4*, 17913–17932. [CrossRef]
20. Mathur, L.; Namgung, Y.; Kim, H.; Song, S.-J. Recent progress in electrolyte-supported solid oxide fuel cells: A review. *J. Korean Ceram. Soc.* **2023**, *60*, 614–636. [CrossRef]
21. Mansilla, Y.; Arce, M.; Oliver, C.G.; Troiani, H.; Serquis, A. Synthesis and characterization of ZrO_2 and YSZ thin films. *Mater. Today Proc.* **2019**, *14*, 92–95. [CrossRef]
22. Bagchi, B.; Basu, R.N. A simple sol–gel approach to synthesize nanocrystalline 8 mol% yttria stabilized zirconia from metal-chelate precursors: Microstructural evolution and conductivity studies. *J. Alloys Compd.* **2015**, *647*, 620–626. [CrossRef]
23. Preux, N.; Rolle, A.; Vannier, R. Electrolytes and ion conductors for solid oxide fuel cells (SOFCs). In *Functional Materials for Sustainable Energy Applications*; Elsevier: Amsterdam, The Netherlands, 2012; pp. 370–401.
24. Stambouli, A.B.; Traversa, E. Solid oxide fuel cells (SOFCs): A review of an environmentally clean and efficient source of energy. *Renew. Sustain. Energy Rev.* **2002**, *6*, 433–455. [CrossRef]
25. Yang, M.; Liu, Y.; Sun, J.; Zhang, S.; Liu, X.; Luo, J. Integration of partially phosphatized bimetal centers into trifunctional catalyst for high-performance hydrogen production and flexible Zn-air battery. *Sci. China Mater.* **2022**, *65*, 1176–1186. [CrossRef]
26. Sun, C.; Hui, R.; Roller, J. Cathode materials for solid oxide fuel cells: A review. *J. Solid State Electrochem.* **2010**, *14*, 1125–1144. [CrossRef]
27. Chen, S.; Zhang, H.; Yao, C.; Lou, H.; Chen, M.; Lang, X.; Cai, K. Review of SOFC Cathode Performance Enhancement by Surface Modifications: Recent Advances and Future Directions. *Energy Fuels* **2023**, *37*, 3470–3487. [CrossRef]

28. Ali, A.; Irshad, M.; Siraj, K.; Raza, R.; Rafique, A.; Ullah, M.K.; Usman, A.; Tiwari, P.; Zhu, B.; Ali, A. A Brief Description of High Temperature Solid Oxide Fuel Cell's Operation, Materials, Design, Fabrication Technologies and Performance. *Appl. Sci.* **2016**, *6*, 75. [CrossRef]
29. Mai, A.; Haanappel, V.A.; Uhlenbruck, S.; Tietz, F.; Stöver, D. Ferrite-based perovskites as cathode materials for anode-supported solid oxide fuel cells: Part I. Variation of composition. *Solid State Ion.* **2005**, *176*, 1341–1350. [CrossRef]
30. Mai, A.; Haanappel, V.; Tietz, F.; Vinke, I.; Stöver, D. Microstructural and electrochemical characterisation of LSFC-based cathodes for anode-supported solid oxide fuel cells. *ECS Proc. Vol.* **2003**, *2003*, 525. [CrossRef]
31. Zhao, L.; He, B.; Lin, B.; Ding, H.; Wang, S.; Ling, Y.; Peng, R.; Meng, G.; Liu, X. High performance of proton-conducting solid oxide fuel cell with a layered PrBaCo2O5+ δ cathode. *J. Power Sources* **2009**, *194*, 835–837. [CrossRef]
32. Lei, L.; Tao, Z.; Hong, T.; Wang, X.; Chen, F. A highly active hybrid catalyst modified $(La_{0.60}Sr_{0.40})_{0.95}Co_{0.20}Fe_{0.80}O_3$-δ cathode for proton conducting solid oxide fuel cells. *J. Power Sources* **2018**, *389*, 1–7. [CrossRef]
33. Zhang, Q.; Hou, Y.; Chen, L.; Wang, L.; Chou, K. Enhancement of electrochemical performance for proton conductive solid oxide fuel cell by 30% GDC-LSCF cathode. *Ceram. Int.* **2022**, *48*, 17816–17827. [CrossRef]
34. Li, G.; He, B.; Ling, Y.; Xu, J.; Zhao, L. Highly active YSB infiltrated LSCF cathode for proton conducting solid oxide fuel cells. *Int. J. Hydrogen Energy* **2015**, *40*, 13576–13582. [CrossRef]
35. Yamaguchi, T.; Shimizu, S.; Suzuki, T.; Fujishiro, Y.; Awano, M. Fabrication and evaluation of a novel cathode-supported honeycomb SOFC stack. *Mater. Lett.* **2009**, *63*, 2577–2580. [CrossRef]
36. Lu, L.; Liu, W.; Wang, J.; Wang, Y.; Xia, C.; Zhou, X.-D.; Chen, M.; Guan, W. Long-term stability of carbon dioxide electrolysis in a large-scale flat-tube solid oxide electrolysis cell based on double-sided air electrodes. *Appl. Energy* **2020**, *259*, 114130. [CrossRef]
37. Li, G.; Gou, Y.; Qiao, J.; Sun, W.; Wang, Z.; Sun, K. Recent progress of tubular solid oxide fuel cell: From materials to applications. *J. Power Sources* **2020**, *477*, 228693. [CrossRef]
38. Nagel, F.P.; Schildhauer, T.J.; Biollaz, S.M.; Wokaun, A. Performance comparison of planar, tubular and Delta8 solid oxide fuel cells using a generalized finite volume model. *J. Power Sources* **2008**, *184*, 143–164. [CrossRef]
39. Timurkutluk, B.; Timurkutluk, C.; Mat, M.D.; Kaplan, Y. A review on cell/stack designs for high performance solid oxide fuel cells. *Renew. Sustain. Energy Rev.* **2016**, *56*, 1101–1121. [CrossRef]
40. Pi, S.-H.; Lee, J.-W.; Lee, S.-B.; Lim, T.-H.; Park, S.-J.; Park, C.-O.; Song, R.-H. Performance and durability of anode-supported flat-tubular solid oxide fuel cells with Ag-Infiltrated cathodes. *J. Nanosci. Nanotechnol.* **2014**, *14*, 7668–7673. [CrossRef] [PubMed]
41. Yang, C.; Jin, C.; Liu, M.; Chen, F. Intermediate temperature micro-tubular SOFCs with enhanced performance and thermal stability. *Electrochem. Commun.* **2013**, *34*, 231–234. [CrossRef]
42. Yoo, Y.; Wang, Y.; Deng, X.; Singh, D.; Legoux, J.-G. Metal supported tubular solid oxide fuel cells fabricated by suspension plasma spray and suspension high velocity oxy-fuel spray. *J. Power Sources* **2012**, *215*, 307–311. [CrossRef]
43. Mahmud, L.; Muchtar, A.; Somalu, M. Challenges in fabricating planar solid oxide fuel cells: A review. *Renew. Sustain. Energy Rev.* **2017**, *72*, 105–116. [CrossRef]
44. Khan, M.Z.; Iltaf, A.; Ishfaq, H.A.; Khan, F.N.; Tanveer, W.H.; Song, R.-H.; Mehran, M.T.; Saleem, M.; Hussain, A.; Masaud, Z. Flat-tubular solid oxide fuel cells and stacks: A review. *J. Asian Ceram. Soc.* **2021**, *9*, 745–770. [CrossRef]
45. Kim, S.-D.; Yu, J.-H.; Seo, D.-W.; Han, I.-S.; Woo, S.-K. Hydrogen production performance of 3-cell flat-tubular solid oxide electrolysis stack. *Int. J. Hydrogen Energy* **2012**, *37*, 78–83. [CrossRef]
46. Muritala, I.K.; Guban, D.; Roeb, M.; Sattler, C. High temperature production of hydrogen: Assessment of non-renewable resources technologies and emerging trends. *Int. J. Hydrogen Energy* **2020**, *45*, 26022–26035. [CrossRef]
47. Minh, N.Q. Solid oxide fuel cell technology—Features and applications. *Solid State Ion.* **2004**, *174*, 271–277. [CrossRef]
48. Steele, B.C.; Heinzel, A. Materials for fuel-cell technologies. *Nature* **2001**, *414*, 345–352. [CrossRef]
49. Klotz, D.; Butz, B.; Leonide, A.; Hayd, J.; Gerthsen, D.; Ivers-Tiffée, E. Performance enhancement of SOFC anode through electrochemically induced Ni/YSZ nanostructures. *J. Electrochem. Soc.* **2011**, *158*, B587. [CrossRef]
50. Chao, C.-C.; Hsu, C.-M.; Cui, Y.; Prinz, F.B. Improved solid oxide fuel cell performance with nanostructured electrolytes. *ACS Nano* **2011**, *5*, 5692–5696. [CrossRef] [PubMed]
51. Zhou, Y.; Wu, H.; Luo, T.; Wang, J.; Shi, Y.; Xia, C.; Wang, S.; Zhan, Z. A Nanostructured Architecture for Reduced-Temperature Solid Oxide Fuel Cells. *Adv. Energy Mater.* **2015**, *5*, 1500375. [CrossRef]
52. Carneiro, J.S.A.; Brocca, R.A.; Lucena, M.L.R.S.; Nikolla, E. Optimizing cathode materials for intermediate-temperature solid oxide fuel cells (SOFCs): Oxygen reduction on nanostructured lanthanum nickelate oxides. *Appl. Catal. B Environ.* **2017**, *200*, 106–113. [CrossRef]
53. Ju, J.; Xie, Y.; Wang, Z.; Zhang, Y.; Xia, C. Electrical performance of nano-structured $La_{0.6}Sr_{0.4}Co_{0.2}Fe_{0.8}O_3$-δ impregnated onto yttria-stabilized zirconia backbone. *J. Electrochem. Soc.* **2016**, *163*, F393. [CrossRef]
54. Celikbilek, O.; Thieu, C.-A.; Agnese, F.; Calì, E.; Lenser, C.; Menzler, N.H.; Son, J.-W.; Skinner, S.J.; Djurado, E. Enhanced catalytic activity of nanostructured, A-site deficient $(La_{0.7}Sr_{0.3})_{0.95}(Co_{0.2}Fe_{0.8})O_{3-\delta}$ for SOFC cathodes. *J. Mater. Chem. A* **2019**, *7*, 25102–25111. [CrossRef]
55. Lee, K.T.; Wachsman, E.D. Role of nanostructures on SOFC performance at reduced temperatures. *Mrs Bull.* **2014**, *39*, 783–791. [CrossRef]
56. Kim, S.-D.; Lee, J.-J.; Moon, H.; Hyun, S.-H.; Moon, J.; Kim, J.; Lee, H.-W. Effects of anode and electrolyte microstructures on performance of solid oxide fuel cells. *J. Power Sources* **2007**, *169*, 265–270. [CrossRef]

57. Tanner, C.W.; Fung, K.Z.; Virkar, A.V. The effect of porous composite electrode structure on solid oxide fuel cell performance: I. theoretical analysis. *J. Electrochem. Soc.* **1997**, *144*, 21. [CrossRef]
58. Kornely, M. *Elektrische Charakterisierung und Modellierung von Metallischen Interkonnektoren (MIC) des SOFC-Stacks*; KIT Scientific Publishing: Karlsruhe, Germany, 2014.
59. Liu, M.; Lynch, M.E.; Blinn, K.; Alamgir, F.M.; Choi, Y. Rational SOFC material design: New advances and tools. *Mater. Today* **2011**, *14*, 534–546. [CrossRef]
60. Karuppiah, K.; Ashok, A.M. *Review of Proton-and Oxide-Ion-Conducting Perovskite Materials for SOFC Applications*; Thomas Telford Ltd.: London, UK, 2019.
61. Yatoo, M.A.; Seymour, I.D.; Skinner, S.J. Neutron diffraction and DFT studies of oxygen defect and transport in higher-order Ruddlesden–Popper phase materials. *RSC Adv.* **2023**, *13*, 13786–13797. [CrossRef] [PubMed]
62. Nikonov, A.; Kuterbekov, K.; Bekmyrza, K.Z.; Pavzderin, N. A brief review of conductivity and thermal expansion of perovskite-related oxides for SOFC cathode. *Eurasian J. Phys. Funct. Mater.* **2018**, *2*, 274–292. [CrossRef]
63. Tanveer, W.H.; Iwai, H.; Yu, W.; Pandiyan, A.; Ji, S.; Lee, Y.H.; Lee, Y.; Yaqoob, K.; Cho, G.Y.; Cha, S.W. Experimentation and modelling of nanostructured nickel cermet anodes for submicron SOFCs fuelled indirectly by industrial waste carbon. *J. Mater. Chem. A* **2018**, *6*, 11169–11179. [CrossRef]
64. Halinen, M.; Saarinen, J.; Noponen, M.; Vinke, I.; Kiviaho, J. Experimental analysis on performance and durability of SOFC demonstration unit. *Fuel Cells* **2010**, *10*, 440–452. [CrossRef]
65. Weber, A.; Dierickx, S.; Kromp, A.; Ivers-Tiffée, E. Sulfur poisoning of anode-supported SOFCs under reformate operation. *Fuel Cells* **2013**, *13*, 487–493. [CrossRef]
66. Hagen, A. Sulfur poisoning of the water gas shift reaction on anode supported solid oxide fuel cells. *J. Electrochem. Soc.* **2012**, *160*, F111. [CrossRef]
67. Brightman, E.; Ivey, D.; Brett, D.; Brandon, N. The effect of current density on H_2S-poisoning of nickel-based solid oxide fuel cell anodes. *J. Power Sources* **2011**, *196*, 7182–7187. [CrossRef]
68. Gavrielatos, I.; Drakopoulos, V.; Neophytides, S.G. Carbon tolerant Ni–Au SOFC electrodes operating under internal steam reforming conditions. *J. Catal.* **2008**, *259*, 75–84. [CrossRef]
69. Gong, M.; Liu, X.; Trembly, J.; Johnson, C. Sulfur-tolerant anode materials for solid oxide fuel cell application. *J. Power Sources* **2007**, *168*, 289–298. [CrossRef]
70. Atkinson, A.; Barnett, S.; Gorte, R.J.; Irvine, J.T.S.; McEvoy, A.J.; Mogensen, M.; Singhal, S.C.; Vohs, J. Advanced anodes for high-temperature fuel cells. *Nat. Mater.* **2004**, *3*, 17–27. [CrossRef]
71. Sun, C.; Stimming, U. Recent anode advances in solid oxide fuel cells. *J. Power Sources* **2007**, *171*, 247–260. [CrossRef]
72. Cheng, Z.; Wang, J.-H.; Choi, Y.; Yang, L.; Lin, M.-C.; Liu, M. From Ni-YSZ to sulfur-tolerant anode materials for SOFCs: Electrochemical behavior, in situ characterization, modeling, and future perspectives. *Energy Environ. Sci.* **2011**, *4*, 4380–4409. [CrossRef]
73. Vincent, A.L.; Luo, J.-L.; Chuang, K.T.; Sanger, A.R. Promotion of activation of CH_4 by H_2S in oxidation of sour gas over sulfur tolerant SOFC anode catalysts. *Appl. Catal. B Environ.* **2011**, *106*, 114–122. [CrossRef]
74. Rao, T.P.; Dhar, G.M. *Recent Advances in Basic and Applied Aspects of Industrial Catalysis*; Elsevier Science: Amsterdam, The Netherlands, 1998.
75. Strohm, J.J.; Zheng, J.; Song, C. Low-temperature steam reforming of jet fuel in the absence and presence of sulfur over Rh and Rh–Ni catalysts for fuel cells. *J. Catal.* **2006**, *238*, 309–320. [CrossRef]
76. Nikolla, E.; Schwank, J.; Linic, S. Promotion of the long-term stability of reforming Ni catalysts by surface alloying. *J. Catal.* **2007**, *250*, 85–93. [CrossRef]
77. Nikolla, E.; Schwank, J.; Linic, S. Direct electrochemical oxidation of hydrocarbon fuels on SOFCs: Improved carbon tolerance of Ni alloy anodes. *J. Electrochem. Soc.* **2009**, *156*, B1312. [CrossRef]
78. Nikolla, E.; Schwank, J.; Linic, S. Comparative study of the kinetics of methane steam reforming on supported Ni and Sn/Ni alloy catalysts: The impact of the formation of Ni alloy on chemistry. *J. Catal.* **2009**, *263*, 220–227. [CrossRef]
79. Kan, H.; Lee, H. Sn-doped Ni/YSZ anode catalysts with enhanced carbon deposition resistance for an intermediate temperature SOFC. *Appl. Catal. B Environ.* **2010**, *97*, 108–114. [CrossRef]
80. Kim, H.; Lu, C.; Worrell, W.; Vohs, J.; Gorte, R. Cu-Ni cermet anodes for direct oxidation of methane in solid-oxide fuel cells. *J. Electrochem. Soc.* **2002**, *149*, A247. [CrossRef]
81. Gorte, R.J.; Vohs, J. Novel SOFC anodes for the direct electrochemical oxidation of hydrocarbons. *J. Catal.* **2003**, *216*, 477–486. [CrossRef]
82. Krishnan, V.V.; McIntosh, S.; Gorte, R.J.; Vohs, J.M. Measurement of electrode overpotentials for direct hydrocarbon conversion fuel cells. *Solid State Ion.* **2004**, *166*, 191–197. [CrossRef]
83. Costa-Nunes, O.; Gorte, R.J.; Vohs, J.M. Comparison of the performance of Cu–CeO_2–YSZ and Ni–YSZ composite SOFC anodes with H2, CO, and syngas. *J. Power Sources* **2005**, *141*, 241–249. [CrossRef]
84. Wang, S.-Q.; Geng, J.-H.; Zhao, X.-X.; Xing, Y.-Z. Elevated sintering capability and electrical conductivity of Fe_2O_3-doped $Ce_{0.8}Sm_{0.1}Nd_{0.1}O_{2-\delta}$ as an electrolyte in IT-SOFCs. *Mater. Chem. Phys.* **2023**, *309*, 128345. [CrossRef]

85. Rahumi, O.; Sobolev, A.; Rath, M.K.; Borodianskiy, K. Nanostructured engineering of nickel cermet anode for solid oxide fuel cell using inkjet printing. *J. Eur. Ceram. Soc.* **2021**, *41*, 4528–4536. [CrossRef]
86. Mashola, T.A.; Matthews, T.; Msomi, P.F.; Maxakato, N.W. Novel nanostructured electrocatalysts for fuel cell technology: Design, solution chemistry-based preparation approaches and application. *Nano-Struct. Nano-Objects* **2022**, *29*, 100831. [CrossRef]
87. Yang, Y.; Zhang, Y.; Yan, M. A review on the preparation of thin-film YSZ electrolyte of SOFCs by magnetron sputtering technology. *Sep. Purif. Technol.* **2022**, *298*, 121627. [CrossRef]
88. Xu, D.; Yan, A.; Yang, Y.; Xu, S.; Zhou, Y.; Yang, S.; Lin, W.-F. Fast ion-conductive electrolyte based on a doped $LaAlO_3$ with an amorphous surface layer for low-temperature solid oxide fuel cells. *J. Power Sources* **2023**, *561*, 232723. [CrossRef]
89. Raza, R.; Zhu, B.; Rafique, A.; Naqvi, M.R.; Lund, P. Functional ceria-based nanocomposites for advanced low-temperature (300–600 °C) solid oxide fuel cell: A comprehensive review. *Mater. Today Energy* **2020**, *15*, 100373. [CrossRef]
90. Chen, G.; Sun, W.; Luo, Y.; He, Y.; Zhang, X.; Zhu, B.; Li, W.; Liu, X.; Ding, Y.; Li, Y. Advanced fuel cell based on new nanocrystalline structure $Gd_{0.1}Ce_{0.9}O_2$ electrolyte. *ACS Appl. Mater. Interfaces* **2019**, *11*, 10642–10650. [CrossRef] [PubMed]
91. Shah, M.Y.; Lu, Y.; Mushtaq, N.; Yousaf, M.; Lund, P.D.; Asghar, M.I.; Zhu, B. Designing Gadolinium-doped ceria electrolyte for low temperature electrochemical energy conversion. *Int. J. Hydrog. Energy* **2023**, *48*, 14000–14011. [CrossRef]
92. Pelosato, R.; Cristiani, C.; Dotelli, G.; Latorrata, S.; Ruffo, R.; Zampori, L. Co-precipitation in aqueous medium of $La_{0.8}Sr_{0.2}Ga_{0.8}Mg_{0.2}O_{3-\delta}$ via inorganic precursors. *J. Power Sources* **2010**, *195*, 8116–8123. [CrossRef]
93. Rauf, S.; Hanif, M.B.; Mushtaq, N.; Tayyab, Z.; Ali, N.; Shah, M.Y.; Motola, M.; Saleem, A.; Asghar, M.I.; Iqbal, R. Modulating the energy band structure of the Mg-doped $Sr_{0.5}Pr_{0.5}Fe_{0.2}Mg_{0.2}Ti_{0.6}O_{3-\delta}$ electrolyte with boosted ionic conductivity and electrochemical performance for solid oxide fuel cells. *ACS Appl. Mater. Interfaces* **2022**, *14*, 43067–43084. [CrossRef]
94. Akbar, M.; Qu, G.; Yang, W.; Gao, J.; Yousaf, M.; Mushtaq, N.; Wang, X.; Dong, W.; Wang, B.; Xia, C. Fast ionic conduction and rectification effect of $NaCo_{0.5}Fe_{0.5}O_2$-CeO_2 nanoscale heterostructure for LT-SOFC electrolyte application. *J. Alloys Compd.* **2022**, *924*, 166565. [CrossRef]
95. Li, C.; Shi, H.; Ran, R.; Su, C.; Shao, Z. Thermal inkjet printing of thin-film electrolytes and buffering layers for solid oxide fuel cells with improved performance. *Int. J. Hydrogen Energy* **2013**, *38*, 9310–9319. [CrossRef]
96. Shim, J.H.; Chao, C.-C.; Huang, H.; Prinz, F.B. Atomic layer deposition of yttria-stabilized zirconia for solid oxide fuel cells. *Chem. Mater.* **2007**, *19*, 3850–3854. [CrossRef]
97. Afroze, S.; Reza, M.S.; Amin, M.; Taweekun, J.; Azad, A.K. Progress in nanomaterials fabrication and their prospects in artificial intelligence towards solid oxide fuel cells: A review. *Int. J. Hydrogen Energy* **2024**, *52*, 216–247. [CrossRef]
98. Shu, L.; Sunarso, J.; Hashim, S.S.; Mao, J.; Zhou, W.; Liang, F. Advanced perovskite anodes for solid oxide fuel cells: A review. *Int. J. Hydrogen Energy* **2019**, *44*, 31275–31304. [CrossRef]
99. Hou, J.; Yang, G.; Liu, W. The principles for rationally designing H-SOFC anode active layer. *Mater. Res. Bull.* **2022**, *150*, 111769. [CrossRef]
100. Yildirim, F.; Timurkutluk, C.; Timurkutluk, B. Optimizing infiltration parameters of nanostructured anode electrode in solid oxide fuel cells. *Ceram. Int.* **2023**, *49*, 23642–23653. [CrossRef]
101. Singh, M.; Zappa, D.; Comini, E. NiO-GDC nanowire anodes for SOFCs: Novel growth, characterization and cell performance. *Mater. Adv.* **2022**, *3*, 5922–5929. [CrossRef]
102. Somacescu, S.; Cioatera, N.; Osiceanu, P.; Calderon-Moreno, J.M.; Ghica, C.; Neaţu, F.; Florea, M. Bimodal mesoporous NiO/CeO_2-δ-YSZ with enhanced carbon tolerance in catalytic partial oxidation of methane—Potential IT-SOFCs anode. *Appl. Catal. B Environ.* **2019**, *241*, 393–406. [CrossRef]
103. Shi, N.; Xie, Y.; Yang, Y.; Huan, D.; Pan, Y.; Peng, R.; Xia, C.; Chen, C.; Zhan, Z.; Lu, Y. Infiltrated $Ni_{0.08}Co_{0.02}CeO_{2-x}$@ $Ni_{0.8}Co_{0.2}$ Catalysts for a Finger-Like Anode in Direct Methane-Fueled Solid Oxide Fuel Cells. *ACS Appl. Mater. Interfaces* **2021**, *13*, 4943–4954. [CrossRef] [PubMed]
104. Zhang, W.; Wang, H.; Guan, K.; Meng, J.; Wei, Z.; Liu, X.; Meng, J. Enhanced anode performance and coking resistance by in situ exsolved multiple-twinned Co–Fe nanoparticles for solid oxide fuel cells. *ACS Appl. Mater. Interfaces* **2019**, *12*, 461–473. [CrossRef]
105. Li, H.; Song, Y.; Xu, M.; Wang, W.; Ran, R.; Zhou, W.; Shao, Z. Exsolved alloy nanoparticles decorated ruddlesden–popper perovskite as sulfur-tolerant anodes for solid oxide fuel cells. *Energy Fuels* **2020**, *34*, 11449–11457. [CrossRef]
106. Choolaei, M.; Jakubczyk, E.; Horri, B.A. Synthesis and characterisation of a ceria-based cobalt-zinc anode nanocomposite for low-temperature solid oxide fuel cells (LT-SOFCs). *Electrochim. Acta* **2023**, *445*, 142057. [CrossRef]
107. Ma, B.; Chen, Z.; Lin, Z.; Cheng, L.; Zhou, Y. Nanostructured Mg-doped Mn–Cr spinel oxide cathodes for solid oxide fuel cells with optimized performance. *J. Power Sources* **2023**, *583*, 233580. [CrossRef]
108. Biswas, S.; Kaur, G.; Paul, G.; Giddey, S. A critical review on cathode materials for steam electrolysis in solid oxide electrolysis. *Int. J. Hydrogen Energy* **2023**, *48*, 12541–12570. [CrossRef]
109. Li, F.; Xu, Y.; Wu, Q.; Zhao, D.; Deng, M. SOFC cathode material of $La_{1.2}Sr_{0.8}CoO_{4\pm\delta}$ with a fibrous morphology: Preparation and electrochemical performance. *Int. J. Hydrogen Energy* **2023**, *48*, 3204–3215. [CrossRef]
110. Zhang, S.-L.; Shang, Y.-B.; Li, C.-X.; Li, C.-J. Vacuum cold sprayed nanostructured $La_{0.6}Sr_{0.4}Co_{0.2}Fe_{0.8}O_{3-\delta}$ as a high-performance cathode for porous metal-supported solid oxide fuel cells operating below 600 C. *Mater. Today Energy* **2021**, *21*, 100815. [CrossRef]

111. Farhan, S.; Mohsin, M.; Raza, A.H.; Anwar, R.; Ahmad, B.; Raza, R. Co-doped cerium oxide $Fe_{0.25-x}MnxCe_{0.75}O_{2-\delta}$ as a composite cathode material for IT-SOFC. *J. Alloys Compd.* **2022**, *906*, 164319. [CrossRef]
112. Tang, H.; Gong, Z.; Wu, Y.; Jin, Z.; Liu, W. Electrochemical performance of nanostructured LNF infiltrated onto LNO cathode for $BaZr_{0.1}Ce_{0.7}Y_{0.2}O_{3-\delta}$–based solid oxide fuel cell. *Int. J. Hydrogen Energy* **2018**, *43*, 19749–19756. [CrossRef]